Addendum to the ARGO proposal

The ARGO–YBJ project

Y.H.Tan, H.H.Kuang, Q.Q.Zhu, H.Y.Wang, P.R.Shen, H.Lu, F.Wang, J.L.Zhang, H.M.Zhang, H.H.He, Z.R.Peng, J.Su, X.H.Ma
IHEP, Beijing, China

X.Y.Zhang, N.J.Zhang, B.Y.Cao, M.He, C.R.Wang, J.Y.Li, Y.Fu, F.M.Kong
Shangdong University, Jinan, China

H.W.Guo, X.R.Meng, A.F.Yuan, D.M.Mei, Labaciren, Zhaxisangzhu, Zhaxiciren, Danzengluobu
Tibet University, Lhasa, China

L.R.Sun, Q.K.Yao, K.Z.Bao, X.D.Yue, Y.N.Wei, S.C.Sun, B.Li
Zhengzhou University, Henan, China

H.Y.Jai, Z.Y.Feng, Q.Huang, G.C.Yu
South West Jiaotong University, Chengdu, China

J.Mu, X.Y.Gao, Q.X.Geng, Z.Q.Liu, H.T.Yang, T.J.Zhang
Yunnan University, Kunming, China

P. Bernardini, F. Cesaroni, P. Creti, G. Mancarella, D. Martello, G. Marsella, M. Panareo, C. Pinto, A. Surdo
INFN and Dipartimento di Fisica dell'Università di Lecce, Italy

B. Bartoli, F. Barone, E. Calloni, S. Catalanotti, B. D'Ettorre Piazzoli, T. Di Girolamo, M. Iacovacci, C. Marmolino, L. Milano
INFN and Dipartimento di Fisica dell'Università di Napoli, Italy

G. Di Sciascio, M. Oliviero, G. Severino
Osservatorio Astronomico di Capodimonte, Napoli, Italy

R. Cardarelli, A. Cavaliere, A. Morselli, P. Padovani, E. Reali, R. Santonico, R. Sparvoli
INFN and Dipartimento di Fisica dell'Universita' "Tor Vergata" di Roma, Italy

C. Bacci, S. Bussino, M. De Vincenzi, N. Iucci, M. Parisi, G. Pellizzoni, P. Pistilli, S. Stalio, C. Stanescu, M. Vietri
INFN and Dipartimento di Fisica dell'Università di Roma Tre, Italy

D. Bastieri, G. Sartori, C. Sbarra
INFN and Dipartimento di Fisica dell'Università di Padova, Italy

S.M. Mari
Università della Basilicata, Potenza, Italy

S. Vernetto
Istituto di Cosmogeofisica del CNR and INFN, Torino, Italy

Contents

1 Introduction

This document presents the technical description of the ARGO experiment at the Yanbajing (Tibet) site (ARGO–YBJ[1]). In a previous document: ASTROPARTICLE PHYSICS WITH ARGO[2] the performance of an experiment consisting of a full coverage detector placed at high altitude ($\sim 4300\ m\ a.s.l$) in detecting extensive air showers was described. In that document a complete computation was presented referring to two detector areas $\sim 3600\ m^2$ and $\sim 10,000\ m^2$ on several physics issues that are summarized in the following points:

1) Gamma–astronomy, at a $\sim 100\,GeV$ threshold energy. More than 300 galactic and extragalactic point candidate sources can be continously monitored, with a sensitivity to unidentified sources about 10% of the Crab flux.

2) Diffuse Gamma–Rays from the Galactic plane, molecular clouds and SuperNova Remnants (SNR) at energies $\geq 100\,GeV$ never observed so far.

3) Gamma Ray Burst (GRB) physics, by allowing the extension of the satellite measurements over the full GeV/TeV energy range.

4) $\overline{p}/p$ ratio at energies $300\,GeV \div \sim TeV$ not accessible to satellites, with a sensitivity adequate to distinguish between models of local (galactic) $\overline{p}$ production and models accounting for an extragalactic origin.

5) The primary proton spectrum in the $10 \div 200\,TeV$ region, with sensitivity sufficient to detect a possible change of the slope of the energy spectrum.

6) Sun and Heliosphere physics, including cosmic ray modulations at $10\,GeV$ threshold energy, the continuous monitoring of the large scale structure of the interplanetary magnetic field and high energy gamma and neutron flares from the Sun.

Additional objectives come from using this detector as a traditional EAS array covering the full energy range from 10^{11} to $10^{16}\,eV$. Since the detector provides a high granularity space–time picture of the shower front, detailed study of shower properties as, for instance, multicore–events, time distributions of EAS particles, multifractal structure of particle densities near the core, can be performed with unprecedented resolution. At an altitude $> 4000 m a.s.l.$ the electron size of the shower produced by primaries energies $10^{15} \div 10^{16}\,eV$ around the 'knee' of cosmic ray spectrum is practically independent of their mass. This fact could be exploited to get information about the composition at the knee by measuring other parameters distinguishing showers developed by primaries of different mass.

In the present document we give technical details of the experiment (mechanical lay–out, electronics , gas system etc.) for a detector of $\sim 6500\ m^2$, placed at the Yanbaijing High

[1] YBJ is a short form for the name YanBaJing

[2] This document, unpublished, is available in compressed postscript format via ftp (login *anonymous*) at *pcmdv.fis.uniroma3.it*. File: *pub/argo_c.ps.z*

Altitude Cosmic Ray Laboratory (Tibet) at an altitude of 4300 m a.s.l., and coordinates 30.11^{o}N 90.53^{o}E. The area of about 6500 m^2 has been chosen as a good compromise between sensitivity and complexity and price of the experiment.
In this addendum it is also presented a computation of γ/h separation exploiting the different patterns of the showers induced by γ and hadrons. This method is very effective in hadron background rejection and therefore the γ detection is substantially improved with respect to that obtained in the previous ARGO document.
Finally, to investigate technical and logistic problems concerning the working conditions in the Yanbaijing laboratory, a test consisting in mounting and operating a 50 m^2 RPC carpet in that laboratory has been performed in winter 1998. The results of this test are presented in this document.

2 The detector design and the mechanical lay–out

The ARGO–YBJ detector is a full coverage detector of dimensions $\sim 71 \times 74$ m^2 realised with a single layer of RPC's. The area surrounding the central detector core, up to $\sim 100 \times 100$ m^2, is partially ($\sim 50\%$) instrumented with the same kind of detector (see figure 1). This ring improves the detector performance, enlarging the fiducial area, for the detection of the showers with the core outside the full coverage carpet.
The basic elements of the ARGO–YBJ detector are RPC's of dimensions 125×280 cm^2. Each RPC is allocated in a box $282 \times 128 \times 5$ cm^3. The box is a light (50 kg), self supporting structure consisting of two foam layers with aluminum sheet glued on both surfaces. The box contains the RPC active detector, the pick–up strip and the front end electronics. Front end cards and strips are welded together in a solid mechanical structure and closed inside the box. All the layers are supported by two irons "C" along the 2.8 m side as shown in figure 3. In the same figure the detector stratigraphy is also shown. These self supporting boxes allows a mounting procedure consisting in putting one box nearby the other after the plugging of cables (HV and signal) and gas tubes is completed. On the top of the boxes, a layer of foam (6 cm thick) with Iron sheets (0.5 mm) glued on both sides separates the RPC boxes from a 5mm thick lead radiator (see figure 3).

3 The Building

The construction of the ARGO–YBJ detector will take few (about three) years. The detector will be hosted in a building with a modular structure to permit at the same time either the construction of the building or the RPC installation and data–taking (with a fraction of the apparatus). We propose for the building a modular structure of 12 halls (one hall corresponds to a module) $\sim 7.9 \times 97$ m^2 in dimensions. A sketch of the building is shown in figure 2. The supporting structure of the building consists in rows of pillars whose dimensions must be contained in a section of $20 \times 30 cm^2$ and 250 cm in height. Spacing among pillars along the row is 5.69 m corresponding to the length of two boxes

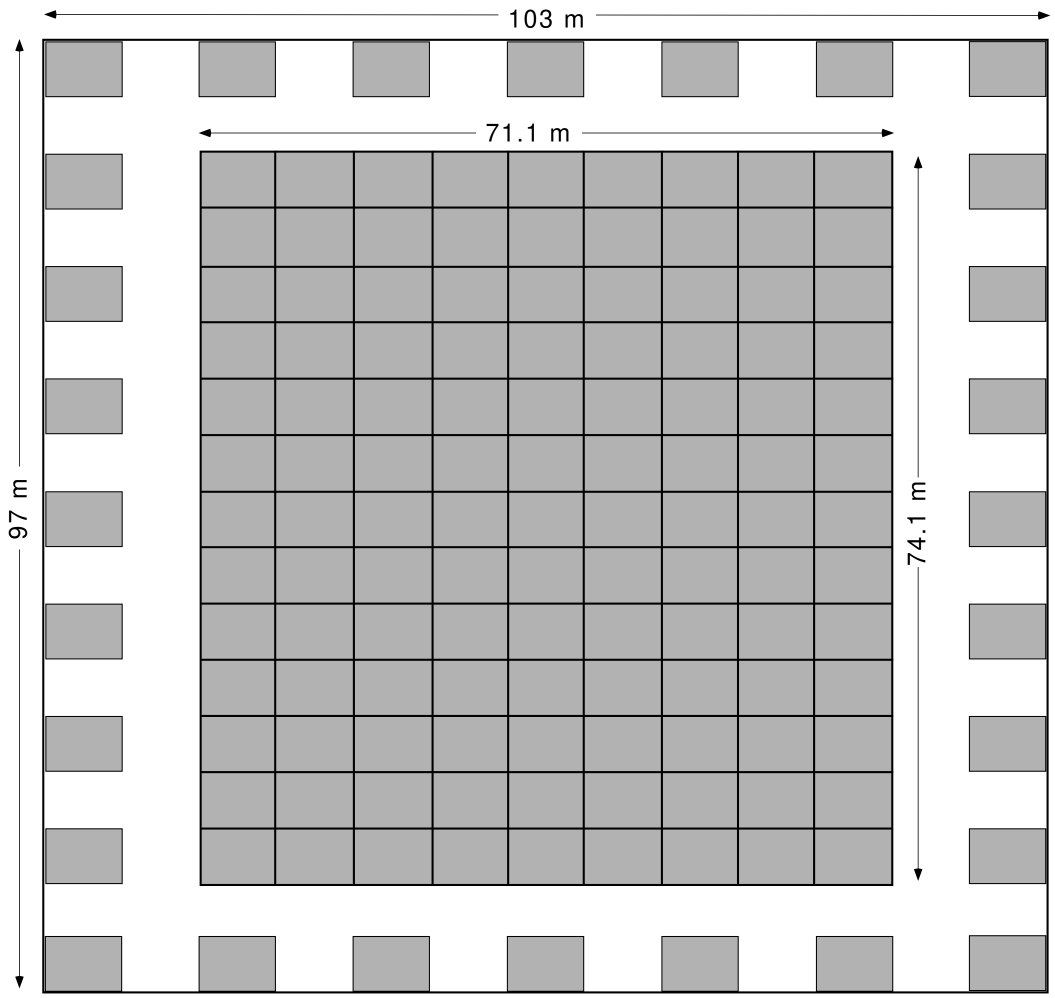

Figure 1: Top view of the ARGO–YBJ detector. The shaded area is the active part of the detector. The rectangles represent a logic subdivision (CLUSTER) of the detector as explained in the text. The detector consists of 117 CLUSTER's in the central part and 28 CLUSTER's in the guard ring for a total of 1740 RPC.

(2.82 m long each) spaced by 5 cm. Inside each hall (7.9 m in width) can fit 6 parallel rows of RPC boxes. As will be clear in the following section these 12 chambers represent a logic unit called CLUSTER whose dimensions are $5.7 \times 7.9\ m^2$. The proposed lay–out allows to achieve a coverage, ratio between active to total area, of about 90%. The first and the last (n. 12) hall will be only partially filled with detectors. The wall of the building will be made out of insulating material in such a way to keep temperature variation as low as possible. In any case the temperature in the experimental hall will be kept in the operating range for the RPC ($\sim 8^o$ to 30^o degrees centigrade).
Near the experimental hall we plan to have a separate building that contains the main control room, the UPS system, a laboratory for the detector maintenance, and, in case, the antenna for satellite communications.
The gases necessary to operate the RPC's will be hosted, for safety reasons, outside the experimental hall in a cabinet, with temperature $T > 5\ ^oC$, to avoid liquefaction of isobutane and freon.

4 Electronics

The detector is organized in modules of 12 chambers as shown in figures 1 and 4. This group of chambers will be referenced in the following as a " CLUSTER". The Trigger and DAQ systems are organized in two levels, Local Stations (LS) that collect and manage the information of one CLUSTER (12 chambers), and Central Station (CS) that collects the information from the local stations and provides the trigger and manages the data collection.

4.1 RPC front-end electronics

The signal pick-up consists of strips 6.7 cm wide 62 cm long glued on one side of 4 mm thick foam sheet. On the other side of the foam sheet an aluminum ground plane is glued. The separation between two adjacent strips is 3.0 mm. The strips are logically organized in pads $56 \times 62\ cm^2$ area. The pads, consisting of 8 strips, are connected to an 8 channel front end electronics board. According to the pad geometry, the resulting strip-line impedance is about 25 Ω.
The front-end electronics is based on an 8-channel discriminator chip which is mounted on boards fixed at the edge of the readout panel [1]. The length of the boards is tuned with the width of the strips so that each board input is essentially in contact with the corresponding strip and no connection wires are required. The input-to-output delay is the same for all the eight channels. Each channel consists of a voltage amplifier connected to a variable-threshold comparator. Figure 5 shows a block scheme of the front-end circuit. It is implemented in a VLSI chip in GaAs technology. The amplifier frequency response is optimized for the typical time structure of the RPC avalanche signal according to the following conditions:

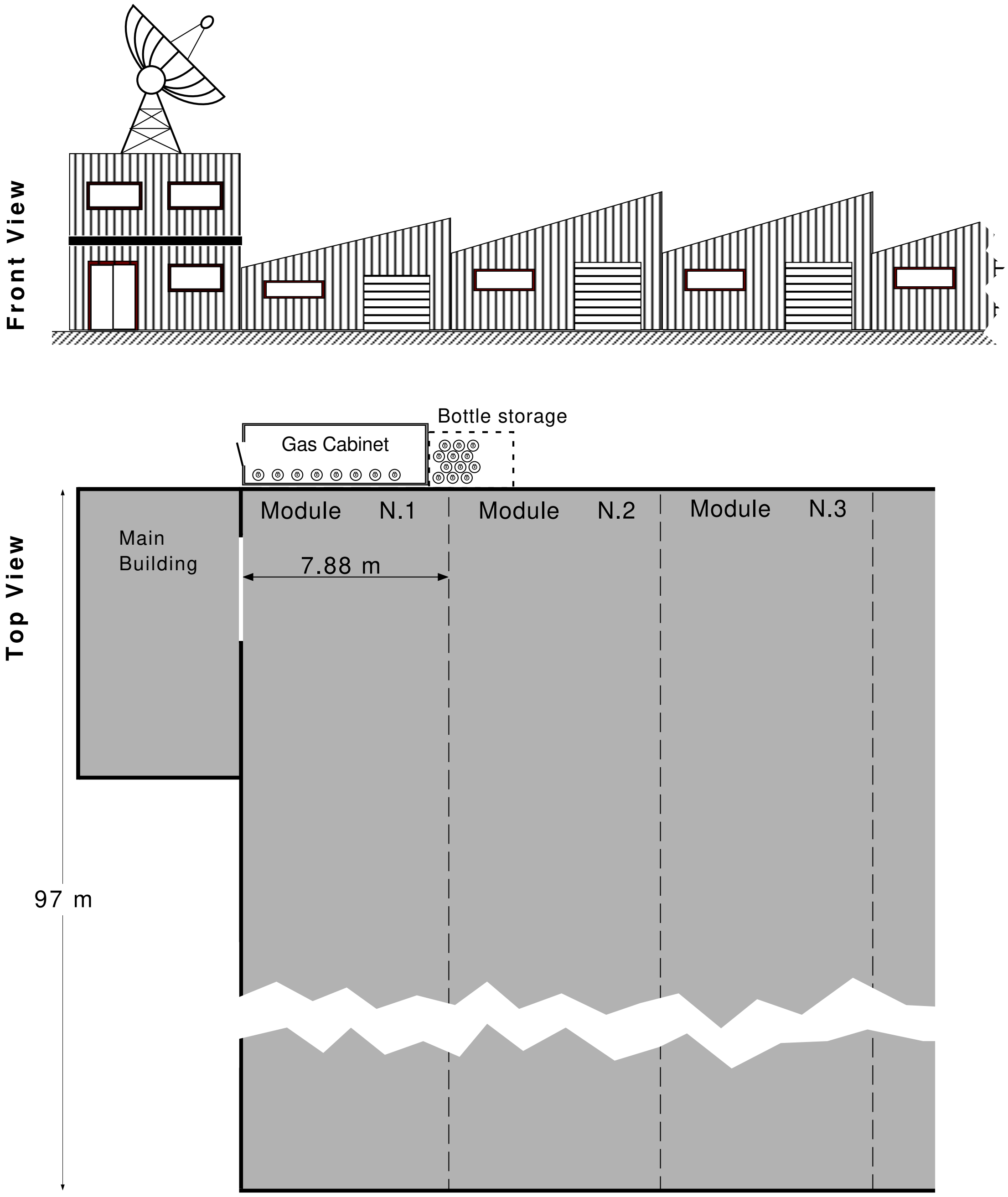

Figure 2: Schematic view of the building (front and top) that hosts the ARGO–YBJ experiment

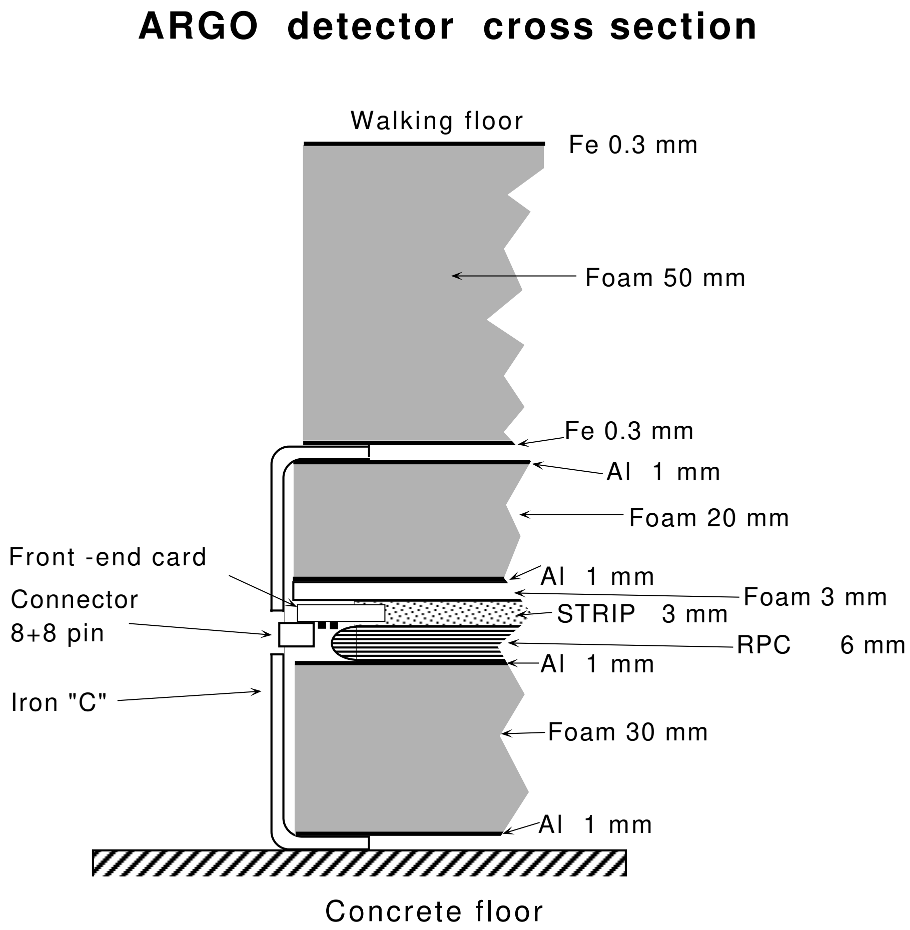

Figure 3: Cross section of the detector

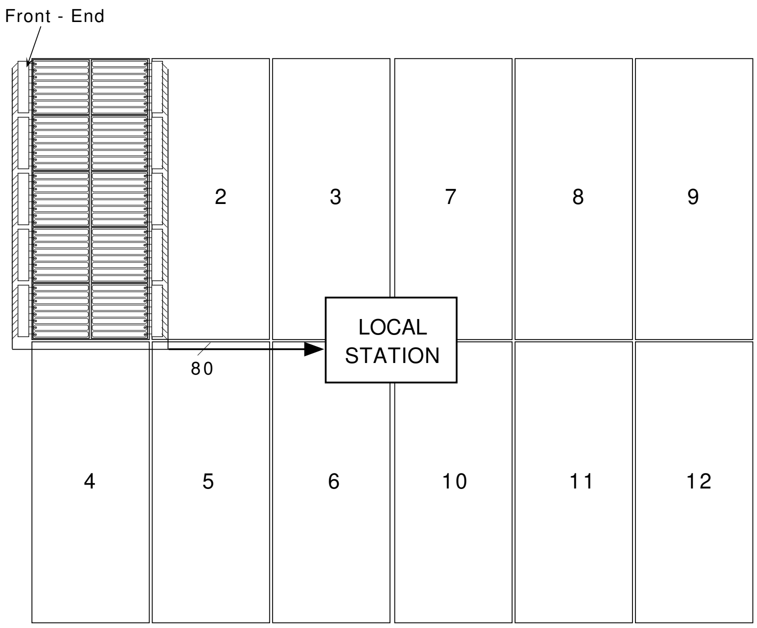

Figure 4: Schematic view of one *CLUSTER* .

- same rise time for the amplified and the input signals;
- minimum return-to-zero time for the output signal.

The amplifier output is bipolar giving zero integrated charge thus avoiding a possible dependence of the steady output voltage on the counting rate. The resulting frequency response has a maximum at 100 MHz and a 3 dB bandwidth of 160 MHz. A two-channel full-custom prototype chip of the front-end circuit has been manufactured in 0.7 mm GaAs technology. This chip, which is a preliminary step before the 8-channel final version, has been successfully tested on board and also mounted on the detector for cosmic ray tests [2]. Electronics specifications are summarized in Table 1. Due to the large range, 50 mV - 2 V, in which the comparator threshold can be fixed, this front end circuit can be used for both avalanche and streamer mode operation of the detector.

4.2 Local Station

This electronics is dedicated to the acquisition of information generated by four groups of three chambers each (in total 120 pads, 8 strips each). This local stations placed on the geometrical center of 6×2 chambers (see figure4), consists of four Signal Processing Cards (SPC) plus one Control and Communication Card (CCC).

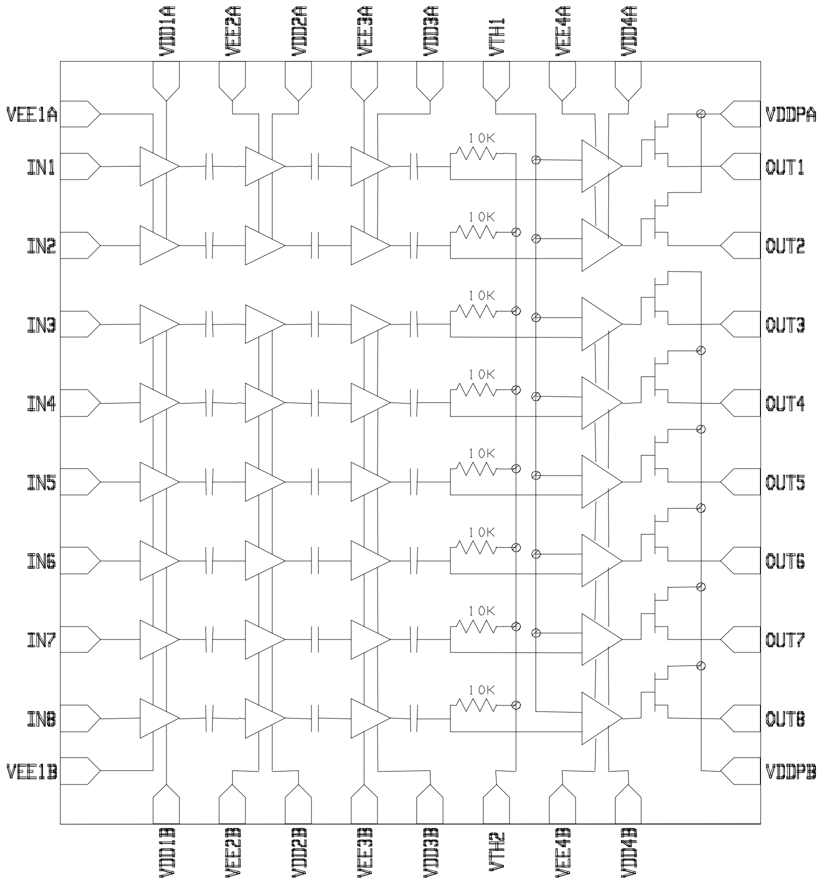

Figure 5: Block scheme of the 8-channel chip front-end amplifier.

Table 1: Electronics specification of the front–end card chip

Maximum rate	100 MHz
Input voltage threshold	0.15 mV
Shaping time	5ns
Time skew	$\leq$ 100 ps
Dissipated power	$\leq$ 30 mW/ch

4.3 Signal Processing Cards (SPC)

Each of the four Signal Processing Cards (SPC) is dedicated to collect and to manage the information generated in three chambers (30 pads) : one 8-twisted-pair cable connects each pads to the SPC; on each twisted pair a $\sim 100\ ns$ pulse is present if one hit occurs on the corresponding strip. For each pad the signals are feed in a receiver chip that performs the FAST OR of the eight signals and store the strip information. The 30 Fast Or signals regarding three chambers are sent to a 32 channels TDC and to a Multiplicity Logic module as shown in figure 6. The TDC [3] has a resolution of $\sim 1\ ns$ and a memory up to 16 time information for each channel. When a "Stop" signal arrives to the TDC, it resets the clock register and it is immediately ready for the acquisition of others hits. Moreover in the TDC it is possible to fix the time window (i.e. $2\mu s$): if the time information regarding one hit exceeds the fixed time window the information is deleted. Also the recorded information of hits generated in the singles strips are deleted after $2\mu s$. The multiplicity logic performs the multiplicity of signals generated in 30 pads. The result has an upper limit of 15 (4 bits): it means that when this limit is reached more than 14 pads have generated signals in a time window equal to the length of pulses ($100ns$).

4.4 Control and Communication Card (CCC)

The CCC performs the multiplicity for one CLUSTER (12 chambers) and sends all the data (time and strip information) to the central station when a trigger is obtained. Moreover the CCC manage the initialization of the TDC's and the masks to kill noisy channels. The multiplicity of 12 chambers is obtained summing the four multiplicity performed by by SPC's. The multiplicity value is maintained on the output for about 300 ns: it is only updated if, in the meanwhile, a greater multiplicity is achieved. The six bits with multiplicity information are continuously sent to the Central station via an 8-twisted pair cable. When a event trigger is generated, the CCC receives a signal. Immediately common stop signals are to the TDC's and then the data transfer is performed. All information (time and strip address) are sent to the central station with zero suppression via a 16-twisted pair cable. All the cables from the local stations to the central station have an equal length of 76 m.

4.5 The Central Station

The Central Station performs the trigger and memorizes the data by dedicated VME modules. The trigger of ARGO–YBJ is based on the CLUSTER's pad multiplicity.
The trigger logic starts to compare the multiplicity M_i of each CLUSTER with three threshold values $M'_{1,2,3}$. In a second step the number of CLUSTER M_{TOTi} that have satisfied the previous conditions is compared with a second group of threshold values $M"_{1,2,3}$. This trigger is realized by means of VME modules.
This scheme permits a record of pad multiplicity on each local group of 12 chambers very useful for the continuous monitoring of the apparatus. When a trigger is obtained a fast signal is sent from the central station to the local station in order to produce common stop to the TDC's and data transfer. It has to be remarked that the delay time from the arrival of the shower front to the common stop signal is less than 2 μs. Therefore we can fix a 2 μs time window on each TDC. In the presence of the trigger all the data recorded within this time window are sent to the central station. The long (2 μs) time window generates a rather large number of spurious hits (~ 12, being 400 Hz the pad rate measured at Yanbajing). These hits can be easily subtracted using the time information during the off–line analysis. The central station consists of VME crates placed in the center of the detector connected with the main control room where the DAQ system will be located. In this way 76 m long cables connecting local and central stations can reach the edges of the apparatus.

5 ARGO–YBJ Data Management

The design and the implementation of an efficient system for the ARGO–YBJ data management is based on make the following considerations:

- **Environment** The location of the detector at the Yanbajing Laboratory requires a more careful design of the electronics of the Data Management System due to the environmental conditions.

- **Data Analysis** The acquired data cannot be sent through the network (with the exception of few relevant frames), because of the small available band. In fact, at the moment a 64 kbit/sec band connection is foreseen. Therefore, a time of one or two weeks is necessary for dispatching the data to the central site in Napoli for the data processing and distribution, both on data summary tapes (DST) and via network.

- **ARGO–YBJ Control** The design of the ARGO–YBJ local control system must take into account the particular location which requires the design of remote control system. Therefore, special techniques should be implemented for the continuous monitoring of the state of the experiment and for all the remote actions on the detector which use the network.

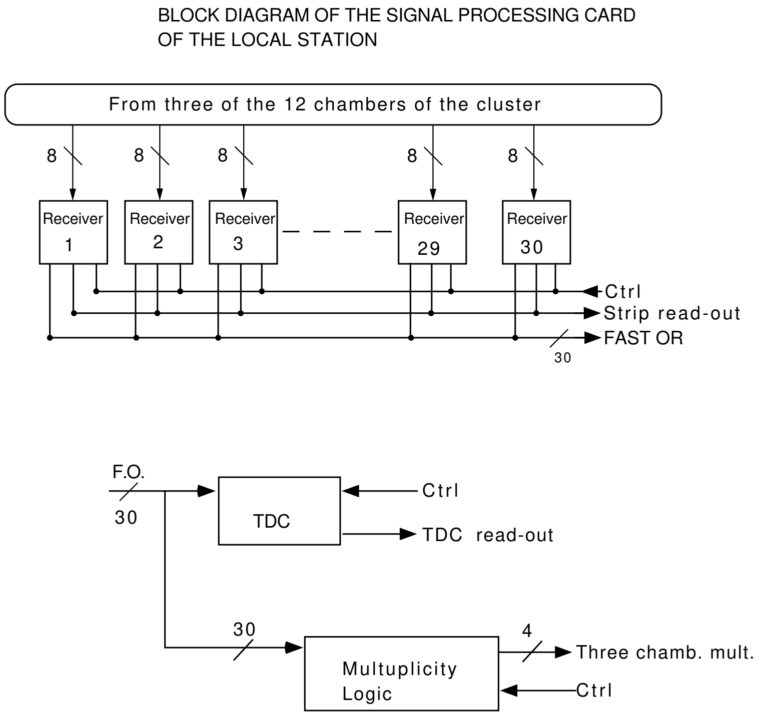

Figure 6: Block Diagram of the SPC

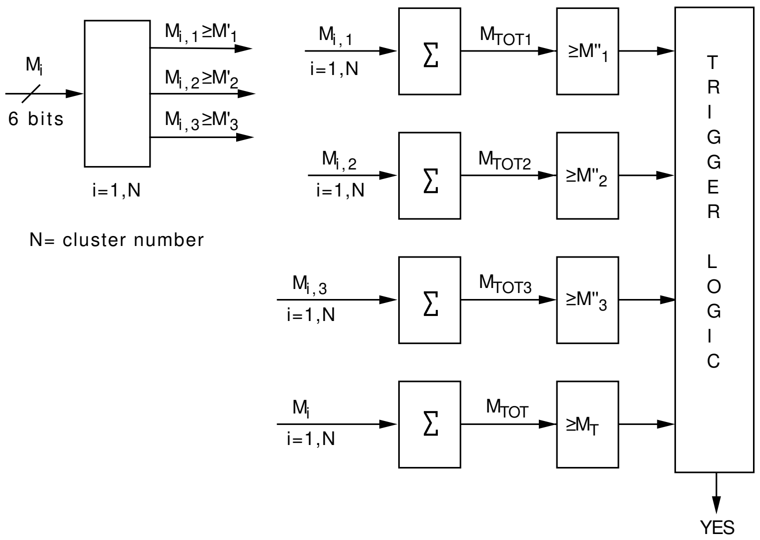

Figure 7: The ARGO–YBJ trigger logic

- **Spare Components** Owing to the difficulty of reaching the laboratory in very short times, a sufficient number of spare parts must be available on site. Effort will be made to reduce as much as possible the number and type of spare parts to be stored at Yangbajing.

5.1 Requirements

The basic requirements for the design and the implementation of the Data Management System are mainly due to the expected data flow. As already described in a previous section of the proposal, the total number of ARGO–YBJ pads is 17400 each with 8 reading strips. All the pads are grouped in clusters, each made of 120 pads. This configuration allows us to define the maximum number of independent acquisition channels which constitute the input of the Data Management System, that is 145 (one channel per cluster).The maximum data flow rate for each input channel of the Data Management System can now be evaluated on the basis of the data structure of the information. This structure consists of two 32-bit words for each pad (8 bytes):

- First word: pad address (16 bit) time information (16 bits)
- Second Word: pad address (16 bit) strips values (on-off) (8 bits)

Therefore, if we assume a dead time equal to 2 μs (due to the transmission time), then the maximum data flow for each channel is 480 Mbyte/sec/channel (Mbyte/sec/cluster). This value can be considered a data flow peak for short times.
On the other hand, the mean data flow for each channel can be evaluated assuming from simulations an event every 200 μs (mean value), that is 5 kHz trigger rate with pad multiplicity $\geq$ 6. This means that we may expect a maximum continuous data flow of 5 Mbyte/sec/channel (Mbyte/sec/cluster), that is 0.8 Gbyte/sec total data flow for the whole system.
Finally, the continuous data flow can be obtained if we assume that only 0.1 - 0.2% of all the pads is firing at the same time. This means that the continuous data flow to be processed and stored by the data acquisition and storage system is 1 Mbyte/sec.
In Table 2 the main requirements of the Data Management System are summarized, including the capacity that the Data Distribution System in Napoli must have in order to be able to manage at least one week of data.

Table 2: **Requirements for the Data Management System**

Parameter	Data Flow	Description
Maximum Data Flow Rate	<480 Mbyte/sec/chan	Peak Data Flow
Maximum Continuous Data Flow Rate	<5 Mbyte/sec/chan	Continuous Data Flow
Data Acquisition Rate	<1 Mbyte/sec	Continuous Data Flow Rate
Data On-line	>500 Gbyte	1 week data

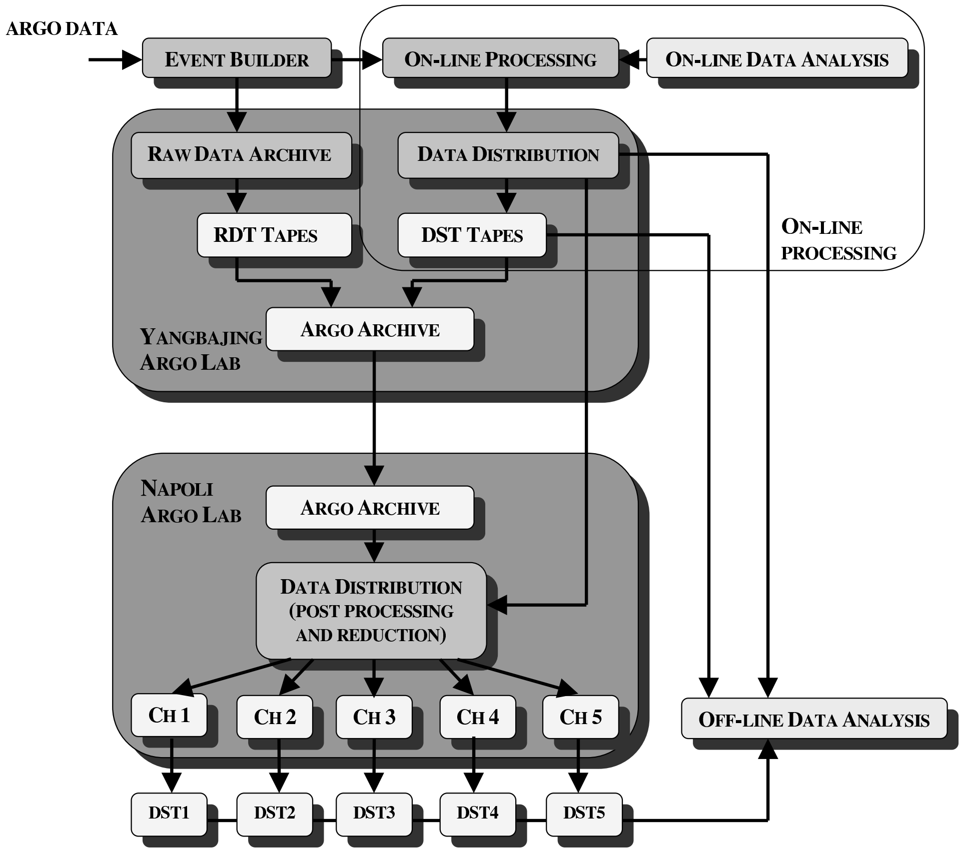

Figure 8: Scheme of the ARGO–YBJ Data Management Architecture

5.2 ARGO–YBJ Data Flow Architecture

The scheme of principle of the Data Flow Architecture is shown in figure 8, where all the main logical links among the systems involved in the data acquisition, archiving and data analysis are shown.
This architecture can be described as follows. The data are sent to the Event Builder through the 145 input channels of the I/O VME boards located on the VME bus of the Event Builder. The Event Builder collects these data and organizes them in frames (including the necessary information on the state of the detector and on the environment). Each frame is the unit information which corresponds to an event and, for this reason, the frame is asynchronous with the timing. Once the Event Builder has built the frame, it sends it to the Raw Data Archiving system which stores them on Raw Data Tapes (RDT). The mean continuous data flow from the Event Builder is about 1 Mbyte/sec, that is about 30 Tbyte/year. According to the state of the technology, it is now possible to use the DLT tapes for data storage, which allow us to store a maximum continuous

data flow of 5 Mbyte/sec on tapes with 35 Gbyte capacity (70 Gbyte in compressed mode). Therefore, on this basis, it is possible to foresee a number of about 1000 (500) DLT tapes/year.
In the Napoli ARGO lab, a Data Distribution system will be implemented whose main job is that of reading the DLT tapes and putting all the frames on-line in such a way that the ARGO labs can have a direct access to the data. The Data Distribution systems also includes a database, which contains all the information about the states on the environment and the ARGO–YBJ experiment.
As an optional possibility, the Event Builder sends the frames to a local On-line Processing System which processes the data and reconstructs on line the events. In such a way the most important frames can be sent in real-time to remote laboratories via network. If we assume a 64 kbit network, then a frame of 1 Mbyte containing interesting events would requires only about 125 sec for being received by the Data Distribution.

5.3 ARGO–YBJ Data Organisation

The ARGO–YBJ data are organised in frames, which are structured units of information containing all the acquired data (raw data), necessary for extracting all the physical information. In particular, each frame is organised as a set of C structures described by a header, and is basically made of three parts (see figure 9):

- structures filled by the Event Builder System, which contain all the collected data (raw data) including all the necessary information on ARGO–YBJ and on the environmental status.
- structures filled by the On-line Processing System, which contain the reconstructed data and all the necessary auxiliary information;
- structures eventually filled by the simulation programs, which are necessary for the comparison of the behaviour of the real detector to the modelled one.

The data organisation in the Data Distribution System is hierarchical for the part related to the frame storage. In fact, the frames selected by the On Line Processing System are stored on the Data Distribution System according to a tree structure and labelled in the same way on RDT, as shown in figure 10.

5.4 Data Management System Architecture

The architecture of the Data Management System is shown in figure 11. This is the typical client/server architecture in which a Supervisor is used to configure and control the whole system. The Supervisor keeps track, requests, allows or inhibits the modifications of the status of this subsystem and can act as Master User Interface.
All the systems can be controlled via a Master User Interface. A special system Error Logger is introduced for collecting all the error messages sent by the Data Management

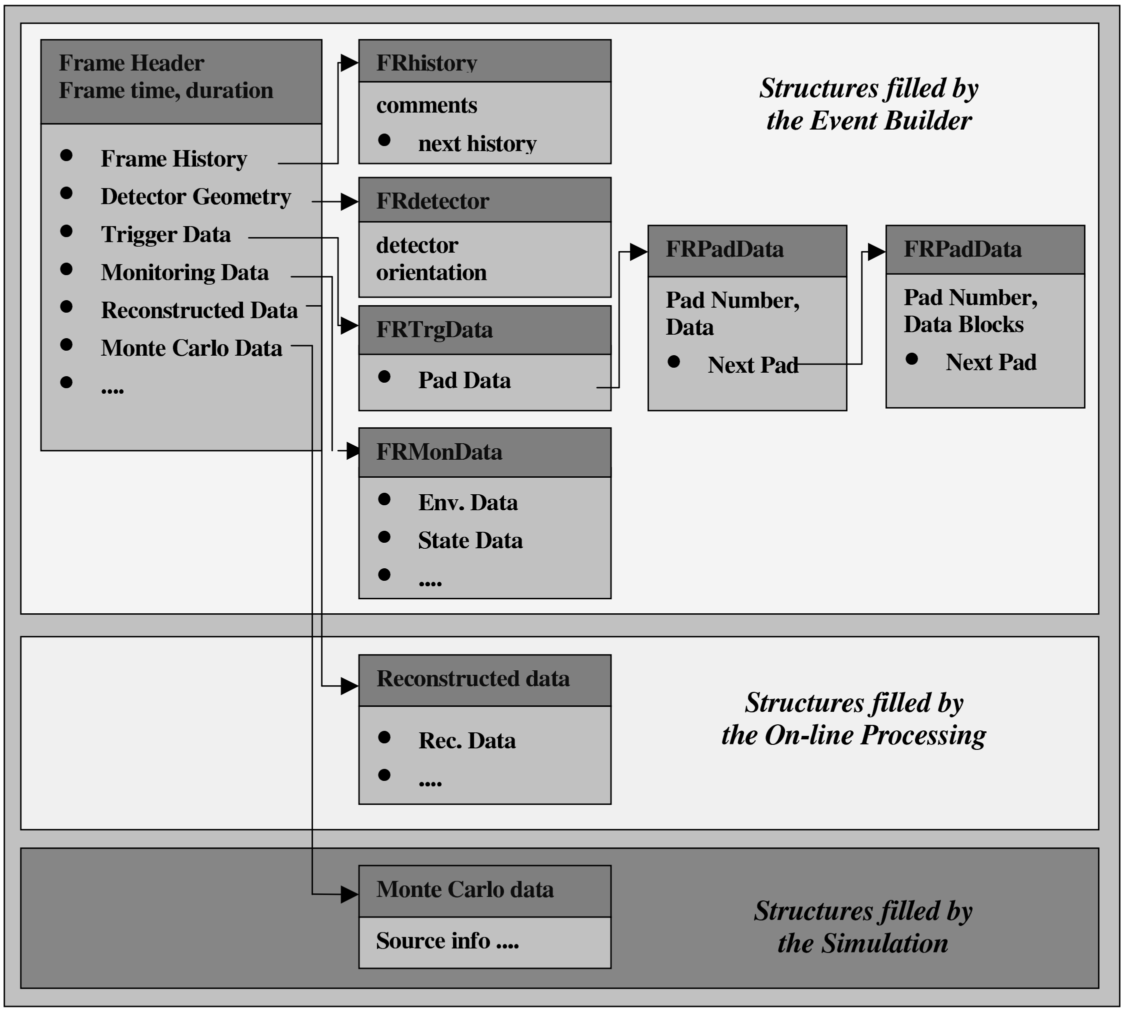

Figure 9: Structure of an ARGO–YBJ Frame

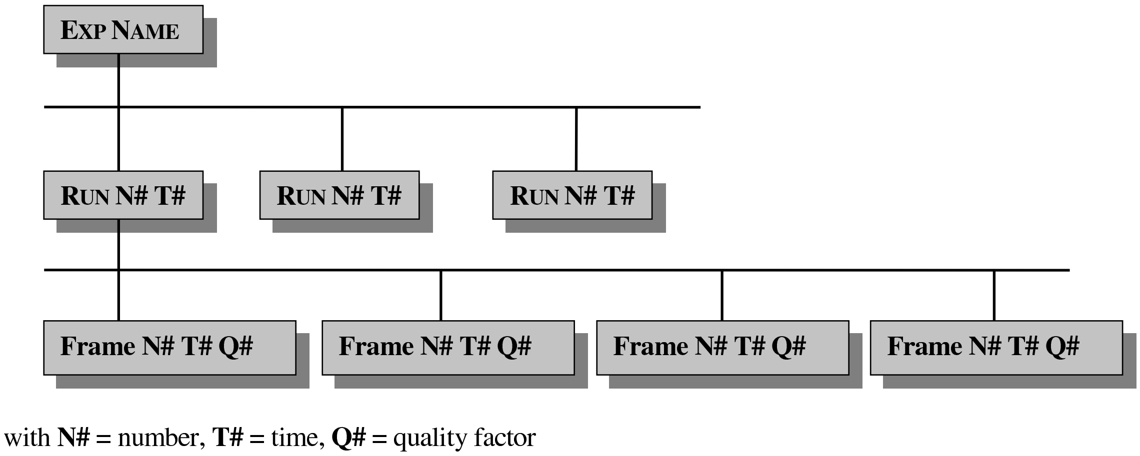

Figure 10: Structure of the Stored Frames in the Data Distribution System

Systems during their normal operation, while an on-line database is introduced for the on-line storage of their configurations.

5.5 Event Builder

The architecture of the Event Builder is shown in figure 12. The Event Builder server is a VME based system in which a master CPU, running the LynxOS operating system, provides the interface among the Event Builder and the Supervisor, the Master User Interface, the Error Logger and the On-Line Database via an Ethernet network. In the VME crate another CPU manages the Event Builder collecting the data coming from the input channels (I/O boards) and preparing and building the frames to be stored in the Raw Data Archive. A memory board (1 Gbyte) is foreseen in order to act as a buffer for all the times in which the amount of data acquired through the I/O boards is larger than the amount that can be stored. The connection among the I/O boards and the memory board is made through a dedicated bus (VSB). All the frames are time labelled using the timing acquired through a VME GPS board. Finally, also the environmental data, acquired through ADC boards, are inserted in the frames.

5.6 Raw Data Archive

The Raw Data Archiving System collects and stores all the frames produced by the Event Builder (raw data). According to the requirements on the continuous data flow rate, the amount of data to be archived is about 86,4 Gbyte/day (1Mbyte/sec data flow rate) on RDT (Raw Data Tapes).
The architecture of the Raw Data Archiving System, shown in figure 13, is the typical

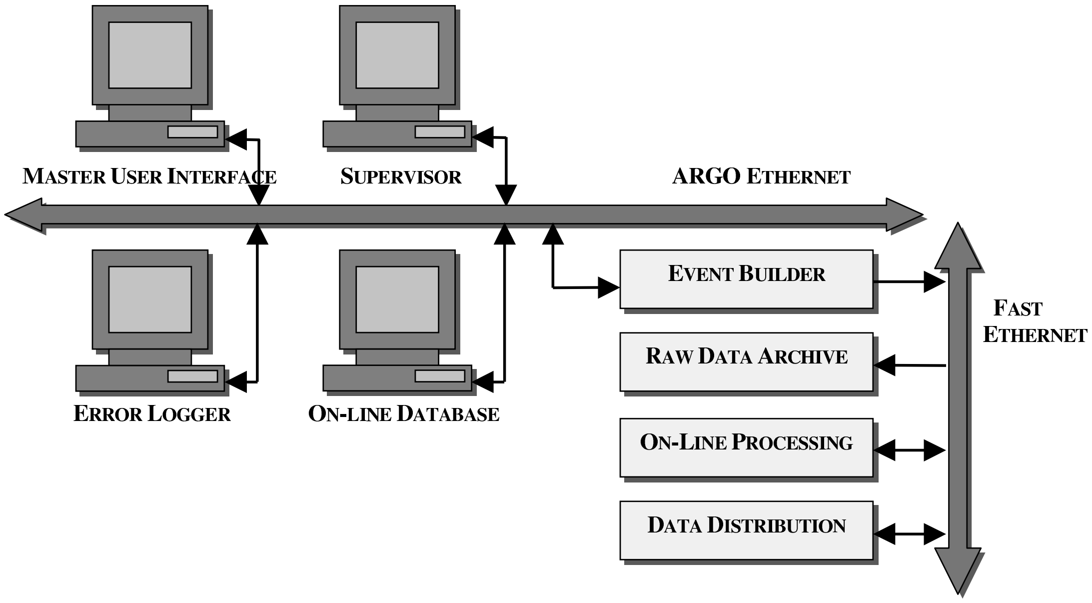

Figure 11: Architecture of the Data Distribution System

client/server architecture, in which the Raw Data Archive (server) is configured and controlled by its User Interface (client). The configuration of the system is stored in the On-line Database while the Error Logger records all the error messages generated the Raw Data Archive. The Supervisor may act as an User Interface.
The matching of the sustained transfer rate (writing mode) of the DLT with the requirement on the data flow and with the restriction of a sequential writing on DLT is obtained by implementing a two stage storage procedure. It consists in a parallel staging of the data on disks (which can sustain a transfer data flow higher than 10 MByte/sec in writing mode and can have a storage capacity up to 18 Gbyte) and then copying the data on DLT. The Raw Data Archiving System is provided with a shadow companion in order to render the system fault tolerant. In this way, the system writes two copies of the archive which will be located in two different places for safety.

5.7 Data Distribution System

The Data Distribution System located in Napoli reads and processes the RDT and stores them on disks (on-line data distribution) an on DST (off-line data distribution). These data contain all the useful information for the off-line data analysis. The system is basically a server running the operating system OSF/1, which mounts all the disks on which the information contained in the DLT tapes will be stored, processed and distributed. A capacity of about 500 Gbyte is foreseen in order to maintain at least 1 week data on line.

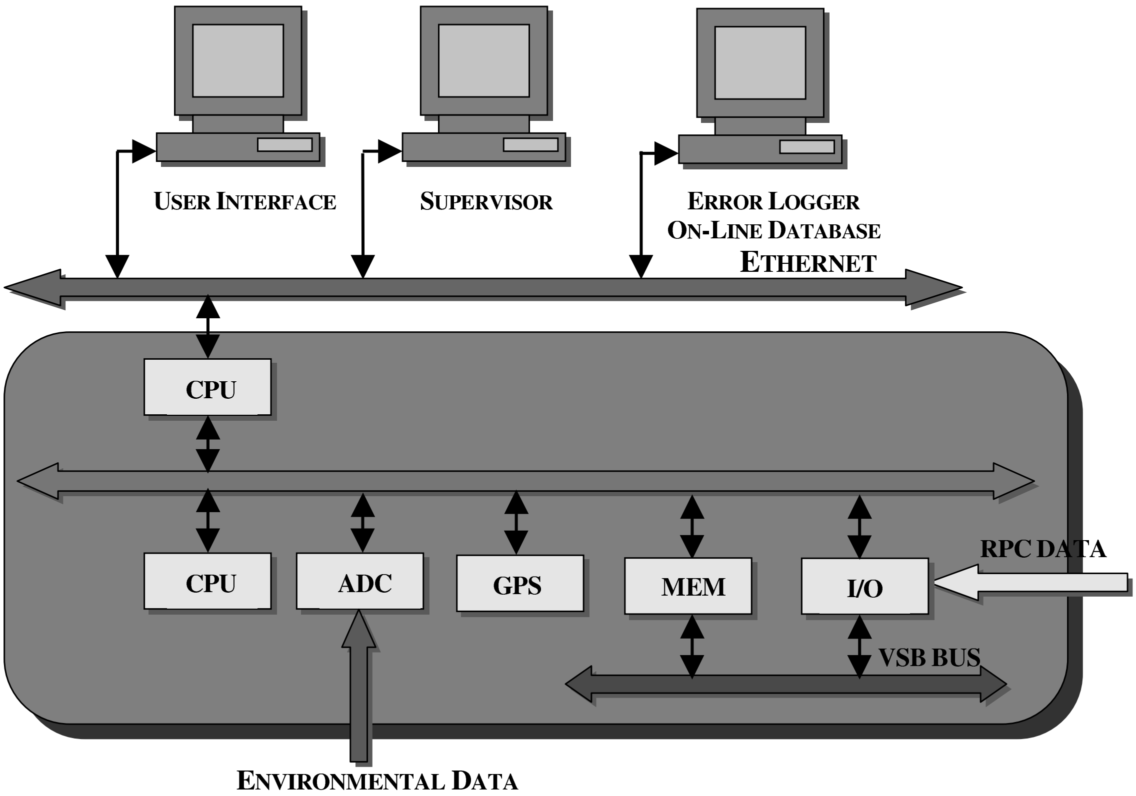

Figure 12: Architecture of the Event Builder

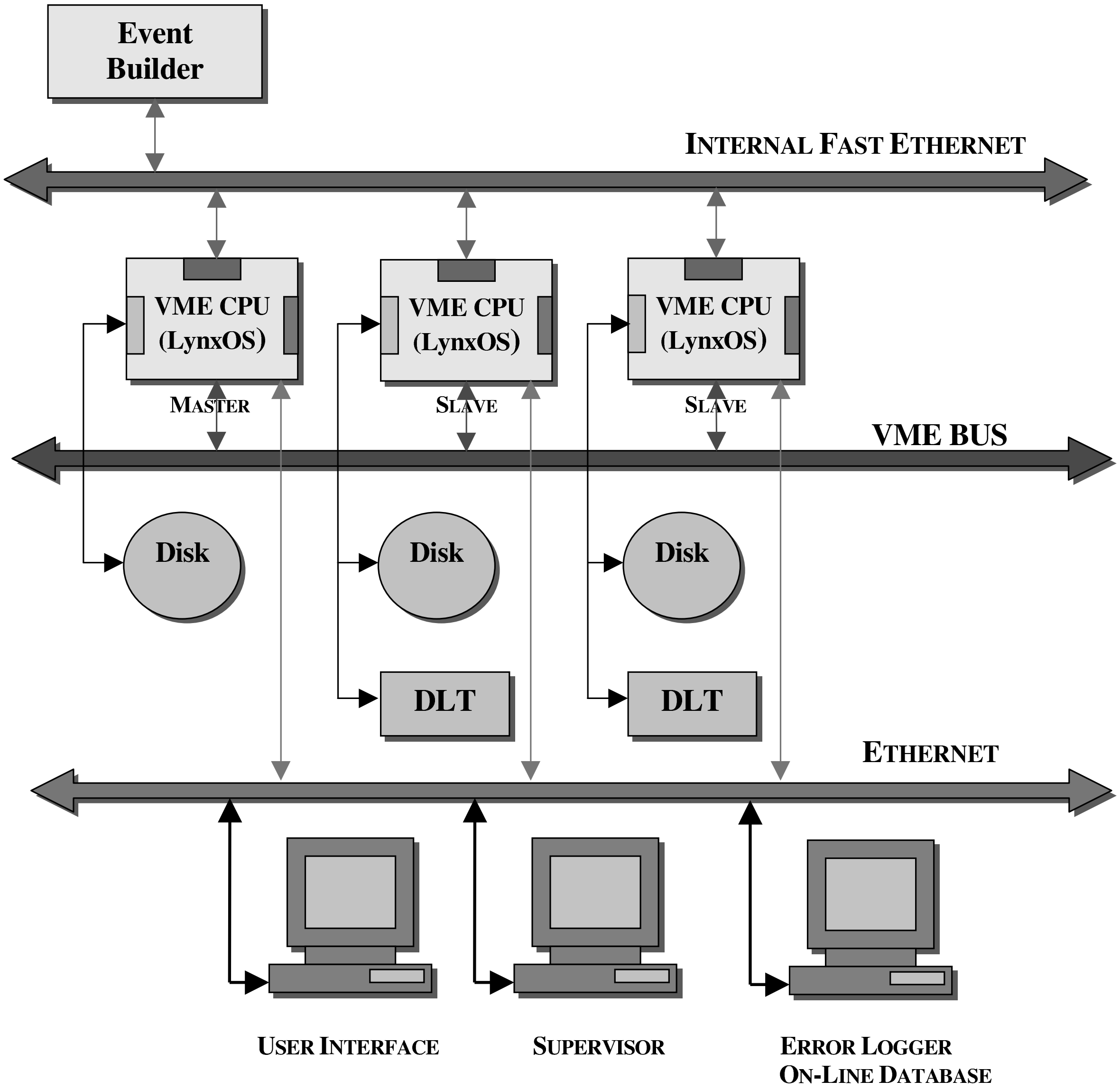

Figure 13: Raw Data Archive System Hardware Architecture

6 Satellite communications and remote control of the experiment

The peculiar geographical position of the experimental site imposes special communication solutions to avoid big delays in detecting and solving possible problems. For the moment we identified as the unique possible solution the use of a satellite borrowed channel with a minimum bandwidth of 64 Kbps. This solution requires the use of a geostationary satellite and the installation of an antenna at the Yanbajing site. The satellite communication system solves also the problem of human communication allowing, within this bandwidth, the voice transmission and the use of "white board" facilities to interactively exchange texts and postscript documents. This bandwidth doesn't allow instead full videoconferencing. As "background" utilization of the satellite channel we foresee the spilling and the transmission of raw events (around 5% of the total event rate) to be reconstructed in the ARGO labs for data quality check. The main application regards instead the LAN to LAN interconnection via the satellite channel permitting the remote control of the Online System. An interactive user interface could be implemented possibly in the frame of the WWW browser to make remote access easier.

7 Gamma–Hadron separation

In order to distinguish between electromagnetic and hadronic showers, the different pattern of the hit distribution in the ARGO–YBJ experimental setup has been used. The particle density profile of the shower front with respect to the core direction is expected to be different in the electromagnetic and hadronic shower: this reflects in a different hit distribution on the apparatus and can be used for a rejection of the hadronic background. We have generated more than 10^4 electromagnetic and hadronic showers in the energy range 50 GeV - 10 TeV, using Corsika code 5.61. The ARGO–YBJ response has been simulated using a Geant-based code, taking into account the ARGO–YBJ layout, inefficiencies and conversion induced by 5 mm thick lead layer. For each event we have reconstructed the shower axis with a dedicated algorithm and we have performed the analysis referring to it as the true shower direction. The Monte Carlo events have been classified according to the number of hits recorded in the apparatus. For each class of events of different hit number, a neural network has been developed to distinguish between photon and hadron induced showers.

Showers have been generated in vertical direction and sampled, between 50 GeV and 10 TeV, from the same energy distribution

$$N(E)dE \ = N_o \ E^{-2.7} dE \qquad (1)$$

The showers simulated in different energy intervals, according to this energy spectrum, are given in the first columns of table 3.

Mean Primary C.R. Energy	Number of simulated showers		Number of detected shower	
(Tev)	*gamma*	*proton*	*gamma*	*proton*
$0.1 < E < 0.5$	110000	110000	82037	25452
$0.5 < E < 1$	5100	5100	5074	3938
$1 < E < 3$	2000	2000	1998	1921
$3 < E < 10$	300	300	300	299
Overall $(0.1 < E < 10)$	117400	117400	89409	31610

Table 3: Number of simulated and detected showers in different energy windows of the primary particle, assuming $\gamma = 2.7$ as spectral index.

In the other two columns of table 3 the number of events which survive to the general cut imposed by the detector thresholds and the trigger logic is shown.

7.1 The neural network

To perform γ/h separation we set up a dedicated neural network that uses as input different variables sensitive to the shower class.
The first variable is the hit distribution of gamma and proton showers. These distributions are shown in figure 14. The second variable used by the neural network is related to the local fluctuations of hit number in each event. This variable $F(x, y)$ is defined as:

$$F(x, y) \ = \frac{|N_{hits}(x, y) - < N_{hits} > |}{\sqrt{< N_{hits} >}} \tag{2}$$

where the mean is computed over the hits of each event.
The third variable used by the neural network is the square of the hit number in each pad. The last variable is the local maximum of the $F(x, y)$ (see eq. 2). These four variables were found particularly sensitive to the differences between gamma and hadron showers. They are used as input to a standard three layers neural network, specifically tuned for our purposes.

7.2 Results on gamma hadron separation

The data sample was classified into different subsets, according to the number of hits in the event. The data sample was processed using half of the available data for net training and the other half to investigate the rejection power of the net. The results, concerning showers generated with core at the center of the carpet, are summarized in table 4, where it is shown the fraction of particle rightly identified, as a function of the hit number. The identification power is about 0.8 for both gamma and proton induced showers, in all the hit ranges we studied.
The results concerning showers generated with the core position located between 20 and 25 meters from the center of the carpet are shown in table 5. The identification power for this sample is about 0.7 for both gamma and proton induced showers.

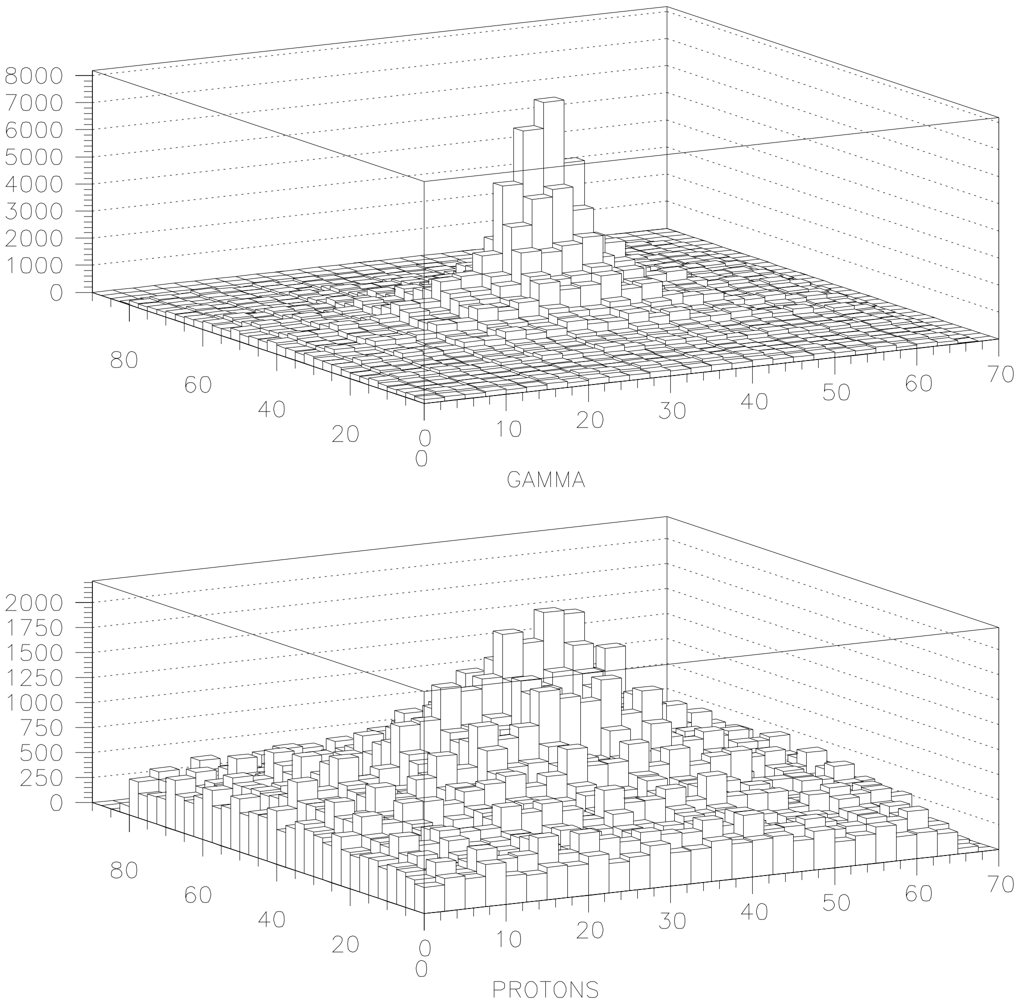

Figure 14: The hit distribution in the ARGO–YBJ detector, for vertical showers with the core at the centre of the carpet, is shown for gamma and proton primaries. Data are averaged over all the generated events.

Hit Number	Total Number of Events	Right Identification ϵ_γ	ϵ_h
$75 < n < 100$	602	0.80	0.70
$100 < n < 150$	788	0.77	0.75
$150 < n < 200$	497	0.85	0.80

Table 4: Identification power ϵ for gamma and proton induced showers generated at the center of the carpet.

The meaning of these results can be expressed in term of the probability that the incoming particle is a gamma (hadron) induced shower, when the network flags it as gamma (hadron). This probability, using the Bayes theorem, can write down in the form:

$$P(\gamma \mid Net = \gamma) = \frac{P(Net = \gamma \mid \gamma)P(\gamma)}{P(Net = \gamma)} \tag{3}$$

where Net is the answer of the neural network. Using the previous equation, we obtain:

$$P(\gamma \mid Net = \gamma) = \frac{\epsilon_\gamma}{\epsilon_\gamma \; + \; (1 - \epsilon_h)\frac{n(h)}{n(\gamma)}} \tag{4}$$

where $n(\gamma)$ and $n(h)$ are the number of gamma and proton induced showers hitting the apparatus.

Hit Number	Total Number of Events	Right Identification ϵ_γ	ϵ_h
$40 < n < 75$	2647	0.73	0.74
$75 < n < 100$	794	0.74	0.71
$100 < n < 150$	792	0.70	0.74
$150 < n < 200$	416	0.65	0.75

Table 5: Identification power ϵ for gamma and proton induced showers with core located between 20 and 25 m from the center of the apparatus.

The rejection power obtained with the neural network can be understood in a more simple and intuitive way. If we consider the number of data detected in a solid angle $\Delta\Omega$ around a given direction, the sensitivity of the apparatus depends on the ratio between the gamma flux $\phi(\gamma)$ and the fluctuation of the hadron shower background flux $\phi(h)$.
With the aid of the neural network rejection, the number of protons is suppressed by a factor $(1 - \epsilon_h)$ (neglecting of course the contribution from the gamma showers), while the gamma signal is reduced by a factor ϵ_γ. Therefore

$$\frac{n(\gamma)}{\sqrt{n(h)}} \simeq \frac{\phi(\gamma)}{\sqrt{\phi(h)}} \frac{\epsilon_\gamma}{\sqrt{(1 - \epsilon_h)}} \sqrt{A^\gamma_{eff} T_{obs} \Delta\Omega} \, R_\gamma \tag{5}$$

where T_{obs} is the observation time, A^γ_{eff} is the effective area for gamma induced showers, and $R_\gamma = \sqrt{A^\gamma_{eff}/A^p_{eff}}$ is a figure–of–merit accounting for the different trigger efficiency for gamma and proton induced showers. The increase of the sensitivity is given by

$$\frac{\epsilon_\gamma}{\sqrt{(1-\epsilon_h)}} \simeq 1.4 \div 1.7 \tag{6}$$

depending on the core position and hit multiplicity. This gain corresponds to the one which could be obtained by means a detector at least two time larger.

8 The sensitivity of a 1200 m^2 ARGO–YBJ detector to GRB's

The ARGO–YBJ full detector will be completed in about 3 years. During the construction time we plane to take data with a fraction of the detector. In this section we discuss the sensitivity of ARGO–YBJ to detect Gamma-Ray-Bursts in the energy range E > 1 GeV, using a detector area of 1200 m^2, that corresponds approximatively to two columns of CLUSTERs as shown in figure 1. To show the effect of the shape of the detector we present the results obtained for two different arrangements:
a) a squared array of 30 × 12 chambers with a total area of 35.1 × 34.2 m^2;
b) a rectangular array of with a total area of 70.2 × 17.1 m^2.
Two different trigger logics can be used to detect photons in the 1 GeV - 1 TeV energy range:
- **trigger 1**: at least 6 pads fired are required;
- **trigger 2**: at least 3 "blocks" are required, where a "block" is one CLUSTER with at least 2 pads fired.
The effective area $A_{eff}(E)$ to detect primary photons and protons with zenith angle θ = 20° is given in figure 15 as a function of the primary energy, for both geometrical arrangements and both trigger types. The squared array combined with trigger 1 has the largest effective areas, in particular at low energy. The calculations are performed for different burst parameters, as time duration, spectrum slope and energy cutoff. The zenith angle of the burst is set to $\theta = 20°$; the sensitivity decreases by increasing θ and the results given here can be considered as averaged values for the θ range $0° - 30°$.
Given a gamma-ray burst with time duration Δt and a photon power-law differential energy spectrum $dS(E)/dE \ = \ K \ E^{-\alpha}$ ph cm^{-2} s^{-1} GeV^{-1} in the energy range 1 GeV < E < E_{max}, the total number of events detected is

$$N \ = \ \epsilon \ \Delta t \int_{1 \ GeV}^{E_{max}} \frac{dS(E)}{dE} \ A_{eff}(E) \ dE \tag{7}$$

where ϵ is the fraction of events from the burst with reconstructed arrival directions inside a circular window centered on the burst position, whose radius ψ depends on the angular resolution of the detector. In the following we use $\epsilon = 0.7$ corresponding to $\psi = 6°$.
The number of events from the burst has to be compared with the background fluctuations. The number of background events recorded during the time Δt from a circular window

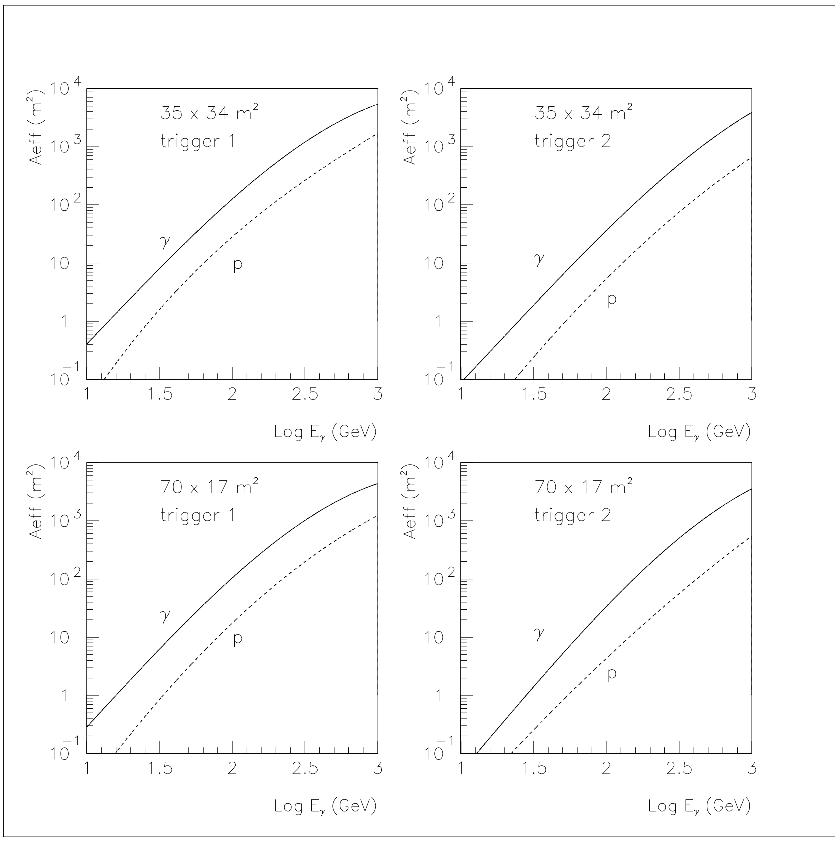

Figure 15: Effective area to detect gamma rays and proton induced showes as a function of the primary energy for two different geometrical arrangement of the detector and two different trigger types.

of radius ψ is given by

$$N_b \ = \ \Delta t \ 2\pi(1 - cos\psi) \int_{E_{p1}}^{E_{p2}} \frac{dS_p(E_p)}{dE_p} \ A^p_{eff}(E_p) \ dE_p \tag{8}$$

where $dS_p(E_p)/dE_p$ is the proton differential spectrum, and $A^p_{eff}(E_p)$ is the effective area for the detection of protons of energy E_p.
The expected rate of background events is 32.9, 9.6, 21.2 and 8.4 s^{-1} respectively for the squared array with trigger 1 and 2 and for the rectangular array with trigger 1 and 2.
Assuming a uniform time distribution of the background, a given gamma-ray burst is detectable if the number N of the events from the burst is significantly larger than the background fluctuations. Requiring the significance of the signal at almost 4 standard deviations, $N \ > \ 4 \ \sqrt{N_b}$, one can evaluate the minimum detectable flux.
The corresponding minimum energy fluence F_{min_0} of a detectable burst in the range 1 Gev - E_{max} is given in figures 16 and 17 as a function of E_{max} for different spectrum slopes α = 1.0, 1.5, 2.0, 2.5, 3.0 and for a burst duration Δt = 1 s. The correspondent value F_{min} for a generic burst of duration Δt, is $F_{min} = F_{min_0} \times \sqrt{\Delta t}$.
The best sensitivity is attained with the squared detector, almost independently on the trigger type. We remark however that the use of trigger 2 is favoured by considering that *i*) the expected background rate is lower than the one associated to trigger 1 *ii*) the short correlation time ($\sim$ 100 ns) required for a 2-pad coincidence in a CLUSTER cuts down the accidental rate to a negligible fraction of the background rate (accidental rate $<$ 0.2 Hz). The sensitivity of the rectangular detector is lower at low energy, but becomes comparable to the squared detector one if E_{max} = 1 TeV.

The recent optical observations of gamma-ray burst afterglows showed that the burst sources are probably located at cosmological distances. In this case a fraction of gamma rays are absorbed in the intergalactic space before reaching the Earth through the $\gamma\gamma \rightarrow e^+e^-$ interaction with low energy photons (cosmic microwave background and infrared radiation field). The absorption entity depends on the photon energy and on the distance of the source. Figure 18 shows a GRB spectrum of slope $\alpha = 2$ affected by the absorption, for different values of the redshift z. We used the absorption coefficients given in [4]. At z=0.1 the absorption is almost negligible, at z=0.5 and z=1.0 the absorption becomes important for photons of energy respectively $>$ 100 GeV and $>$ 50 GeV. From these calculations we find that the sensitivity of this 1200 m^2 carpet, for spectra extending out to 300 GeV and lasting 1 s, is about 7 10^{-6} $erg \cdot cm^{-2}$ for $1 < \alpha < 2$. The absorbtion limits the range from which 300 GeV photons can reach us to about 500 Mpc.
In the following we evaluate how the ARGO–YBJ sensitivity to detect GRBs decreases as a function of their distance. We limit our calculations to the squared array operating with trigger 1 and to GRB spectra with slope $\alpha = 2$ and time duration Δt = 1 s. Figure 19 shows the minimum fluence of a detectable GRB located at different distances. The sensitivity is not strongly affected for GRB spectra with $E_{max} <$ 100 GeV, but is lowered by a factor $\sim$ 10 for spectra extending up to 1 TeV and z = 0.5.

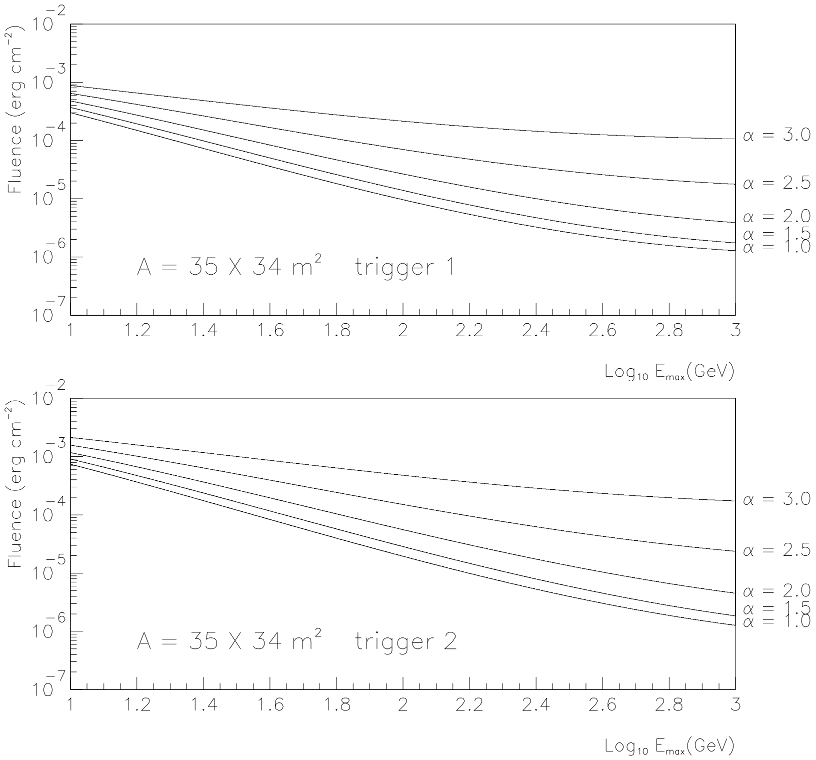

Figure 16: The minimum value F of the energy fluence in the range 1 GeV $< E < E_{max}$, for a detectable burst of time duration $\Delta t = 1$ s, as a function of E_{max}. The burst spectrum is assumed to be a power law one extending in the energy range 1 GeV $< E < E_{max}$. F is given for 5 different values of the spectrum slope α. The curves are calculated for the squared detector and two different trigger types.

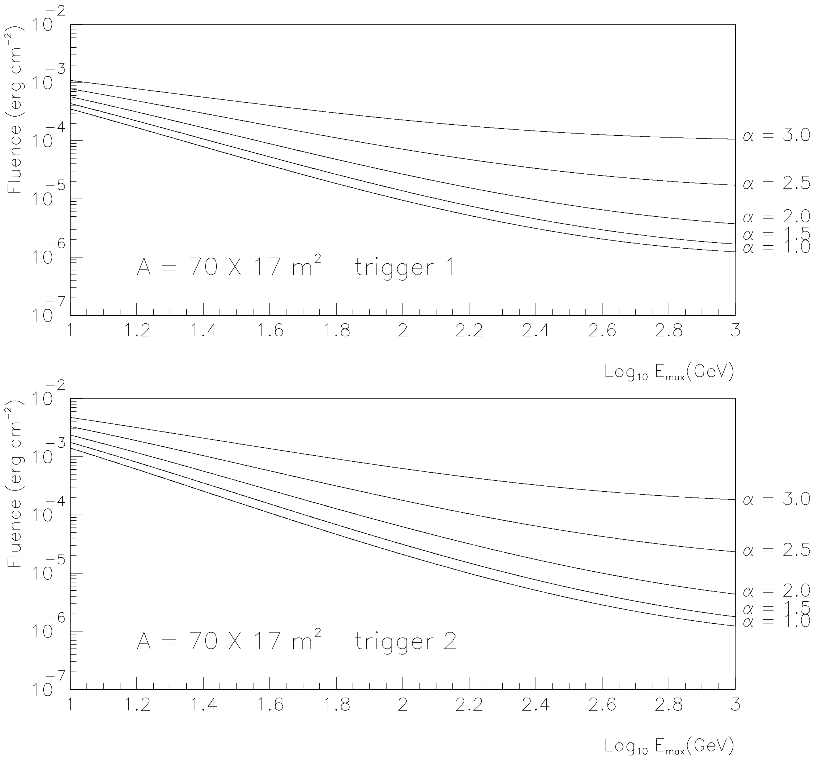

Figure 17: The same as in previous figure for the rectangular detector.

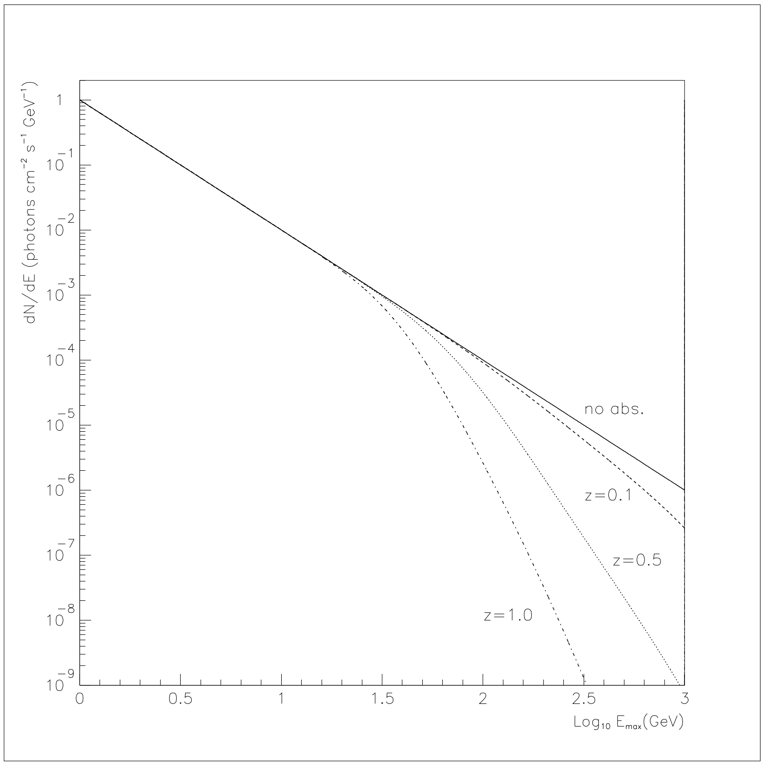

Figure 18: The energy spectrum of a GRB located at different distances from the Earth affected by absorption on the infrared radiation.

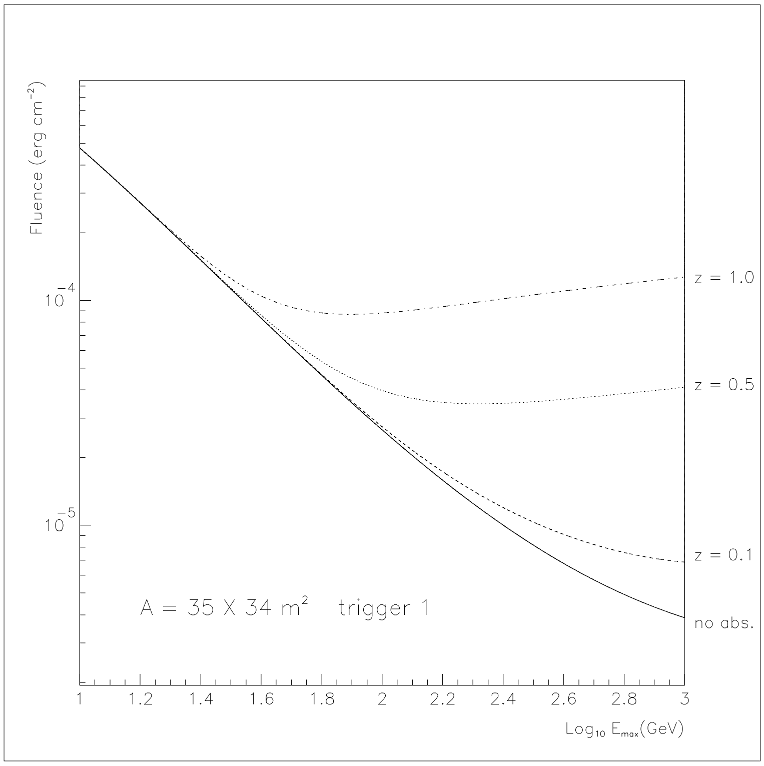

Figure 19: The minimum value F of the energy fluence in the range 1 GeV $< E < E_{max}$, for a detectable burst of time duration $\Delta t = 1$ s and slope $\alpha = 2$, as a function of E_{max}. The curves are given for different values of the redshift of the burst.

9 Results of the test at YBJ

In order to investigate the performance of RPC's operated at 4300 m a.s.l., a full coverage carpet of 50 m^2 area has been installed at YBJ site. It consists of 15 chambers placed in 5 columns, displaced by 10 cm, and 3 rows displaced by 5 cm. The RPC chambers are placed on the ground of a building that contains also the electronics and the DAQ system.

9.1 RPC carpet lay-out

The detector consists of single-gap RPC's, made of bakelite ($\rho > 510^{11}\Omega{\cdot}cm$) $280{\times}112$ cm^2 area. The RPC's read-out is performed by means of Al strips 3.3 cm wide and 56 cm long at the edge of which the front–end electronics is connected. A foam sheet 4 mm thick is glued between the strips and the Aluminum ground plane. The FAST OR of 16 strips defines a logic unit called pad, 10 pads (56×56 cm^2) cover each chamber. The FAST-OR signal from each pad is sent via coaxial cable, to dedicated modules that generate the trigger signal and the STOP signals to the TDC's. Each channel of the TDC's measures, with a time resolution of about 1 ns, the arrival times (up to 16 per channel) of the particles hitting one pad. The trigger logic allows to select events on the base of the pad multiplicity.

9.2 The performance of the RPC's

The RPC's have been operated in streamer mode with gas mixtures based on argon, isobutane and tetrafluoroethane $C_2H_2F_4$, (Freon).
We used different gas mixtures with increasing freon percentages to improve the primary ionization, by keeping the isobutane fraction close to the non flammability limit.
The description of the measurements made on gas mixtures at YBJ is given in section appendix. In figure 20 it is shown a typical curve of the current absorbed by the chambers as a function of the HV for the gas mixture Ar 15%,ISO–B 10% Freon 75% . This mixture has been chosen because provides a smaller contamination of afterpulses. For the same gas mixture, the single rate of the OR of four pads belonging to the same RPC is shown in figure 21 as a function of HV: the curve presents a well defined plateau corresponding to a rate of about 400 Hz per pad.
The plot of figure 22 shows a typical efficiency curve as measured by means of a telescope consisting of three 50×50 cm^2 RPC. The measured efficiency af all the 150 pads of the carpet, turns to be about 94%.
In order to obtain the overall time resolution, we have measured the time difference between the pad signals and the external trigger provided by the telescope.
The RPC's have been operated at 7400 V, about 500 V above the plateau knee. The time distribution of the RPC signals for different pads, are shown in figure 23. Fitting the distribution with a gaussian curve, we obtain a typical resolution of $1.3 \div 1.5$ ns.

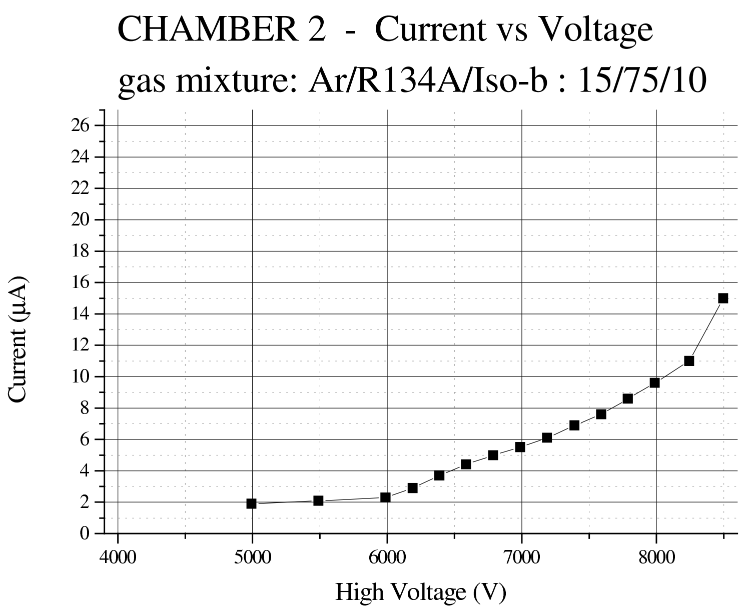

Figure 20: RPC current as a function of High Voltage.

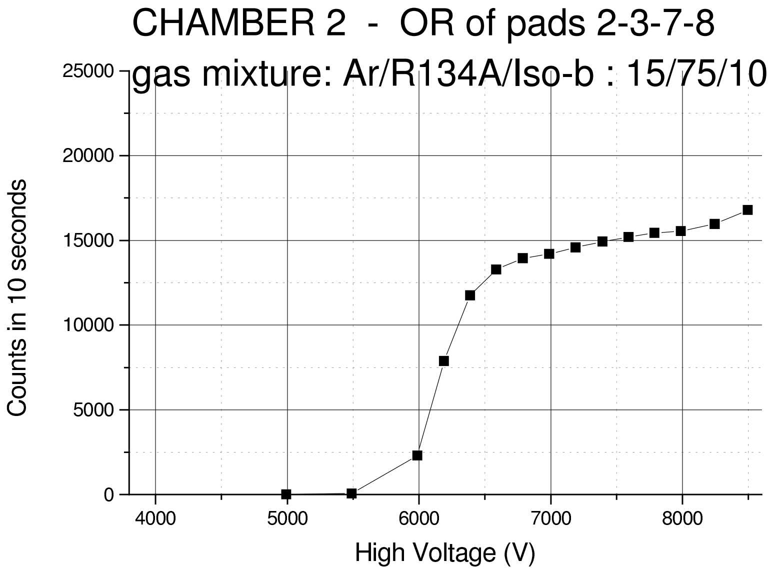

Figure 21: RPC single rate of the four OR-ed pads as function of High Voltage

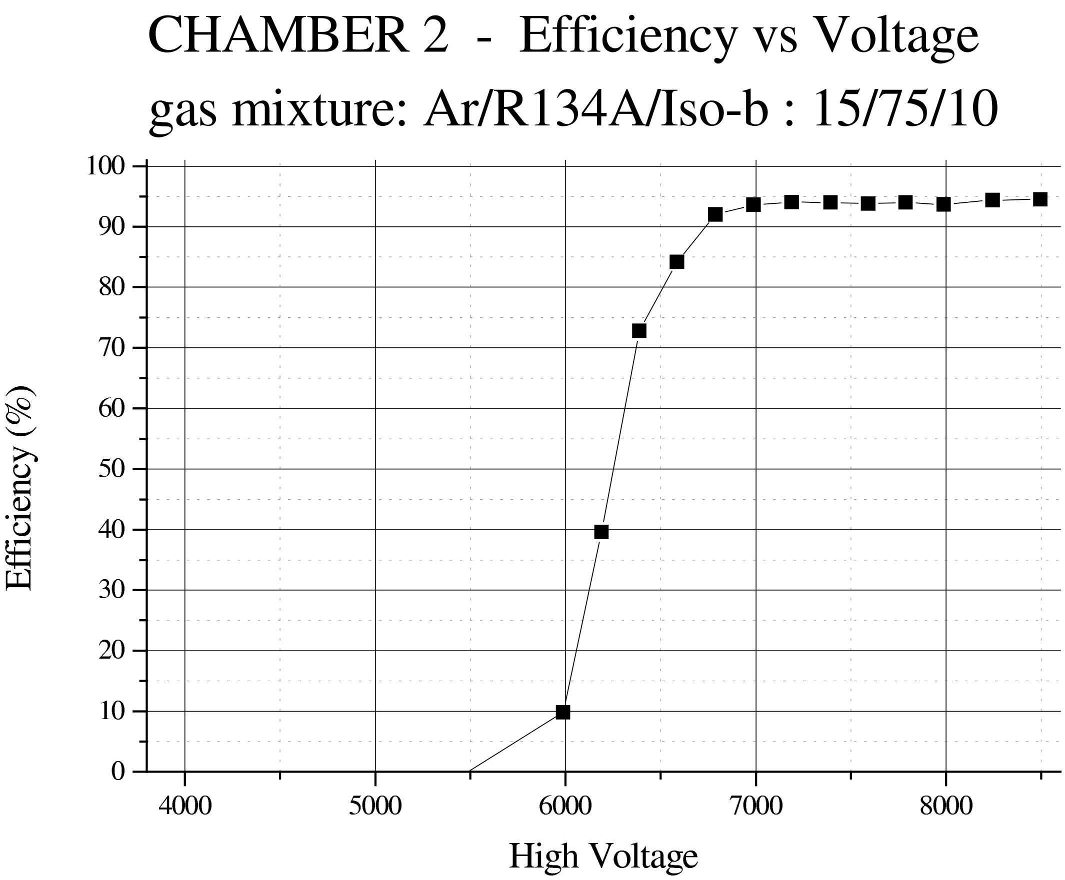

Figure 22: RPC efficiency curve as a function of High Voltage.

This result includes the time spread due to the electronics (front-end, TDC's) and to the length of the strips. The resolution of the electronics alone, measured with a pulser, is $\sim 0.7\ ns$.

9.3 Results from the carpet operation

Data were taken either with or without a 5 mm layer of lead on the whole carpet. Different triggers based on pad multiplicity have been used to collect about 70000 shower events without lead and about 10^6 shower events with lead on the top. They represent a very detailed space–time picture of a small portion of the shower front. In the following we present the results from a preliminary analysis of these data.
The integral rate as function of the pad multiplicity is shown in figure 24 for both conditions. Since the pad rate is about 400 Hz and the pad signal is shaped to 1.5 μs the trigger rate of multiplicity greater then 6 is unaffected by accidentals. A comparison at fixed rate indicates an increasing of the pad multiplicity, due to the effect of the lead as expected according to our simulation.
Events with a pad multiplicity ≥ 30 has been selected to study the time profile of the shower front. In the very good approximation of a planar shape of the shower front the expected arrival time of the particles is a linear function of the position. The time spread around the fitted values gives information on the shower time thickness folded with the detector time resolution.
The time profile observed in one event along aligned pads is shown in figure 25.
The distribution of the residual times with respect to the fitted plane are presented in figures 26, 27 and 28 for three different intervals of pad multiplicity, with and without lead. The effect of the lead consists in a shrinking the time thickness of the shower, since the lead absorbs low energy electrons, which mostly contribute to the tail of the time distribution, and permits the conversion of shower photons.
We have studied the angular distributions of the shower direction hitting the carpet. This direction is obtained as the normal to the plane fitted using the measured arrival times. The results for the theta and the azimuth distributions, are consistent with the expectation. The zenith distribution is shown in the figure 29.
We have studied the angular resolution of the detector by using the chess board method. Events with N pads have been selected according to the constraint N_e(even pads) $\simeq$ N_o(odd pads $\simeq N/2$). The arrival shower direction has been reconstructed for both subsamples. The space angle difference $\Delta\theta$ between these directions is shown in figure 30 for events with $N = 130 \div 140$. The detector angular resolution σ_θ can be estimated by means of the following relation

$$\sigma_\theta = \frac{M_{\Delta\theta}}{1.177 \cdot 2} \tag{9}$$

where $M_{\Delta\theta}$ is the median of the $\Delta\theta$ distribution. From data collected with the lead layer we obtain $\sigma_\theta \simeq 3.8^o$, a factor of 1.5 better than the result obtained without lead.

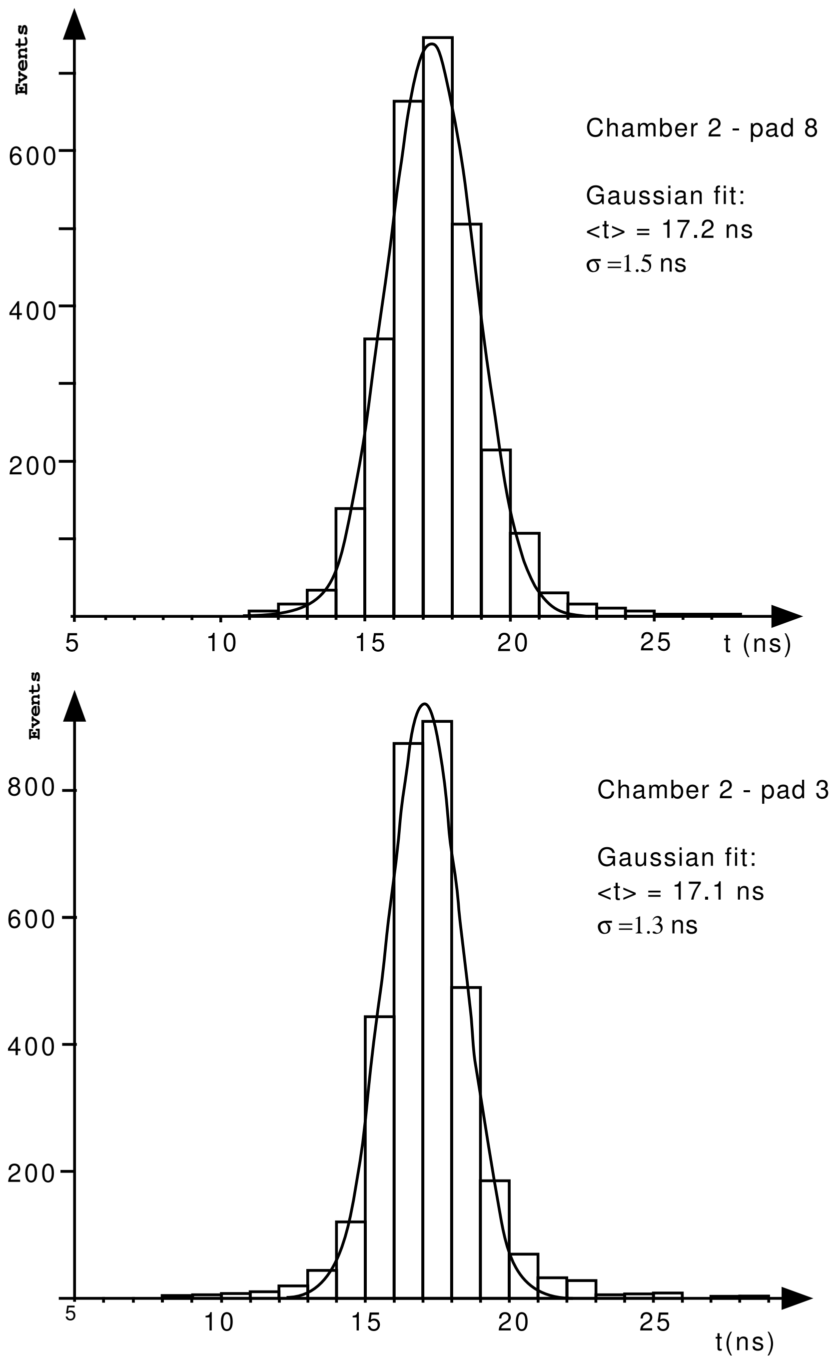

Figure 23: Typical time distribution of pad signals for two different pads.

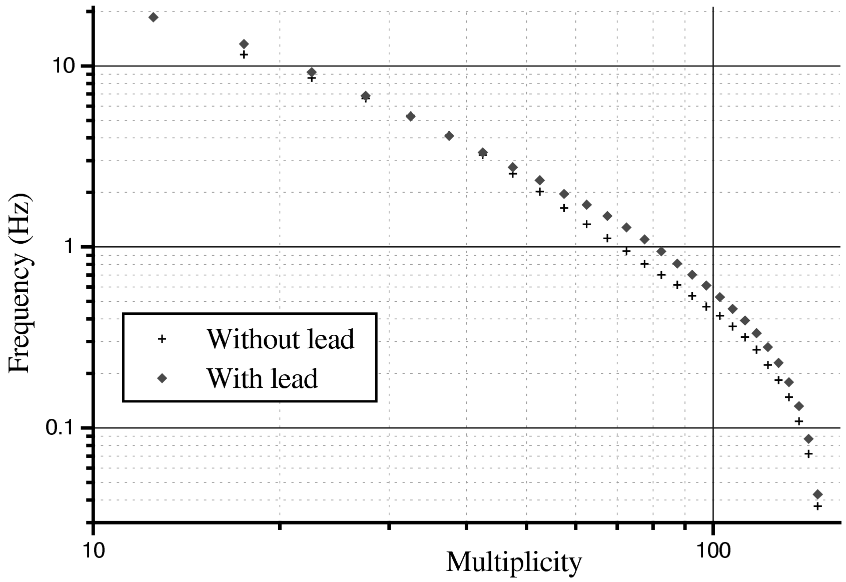

Figure 24: The integral rate as a function of the pad multiplicity with and without lead.

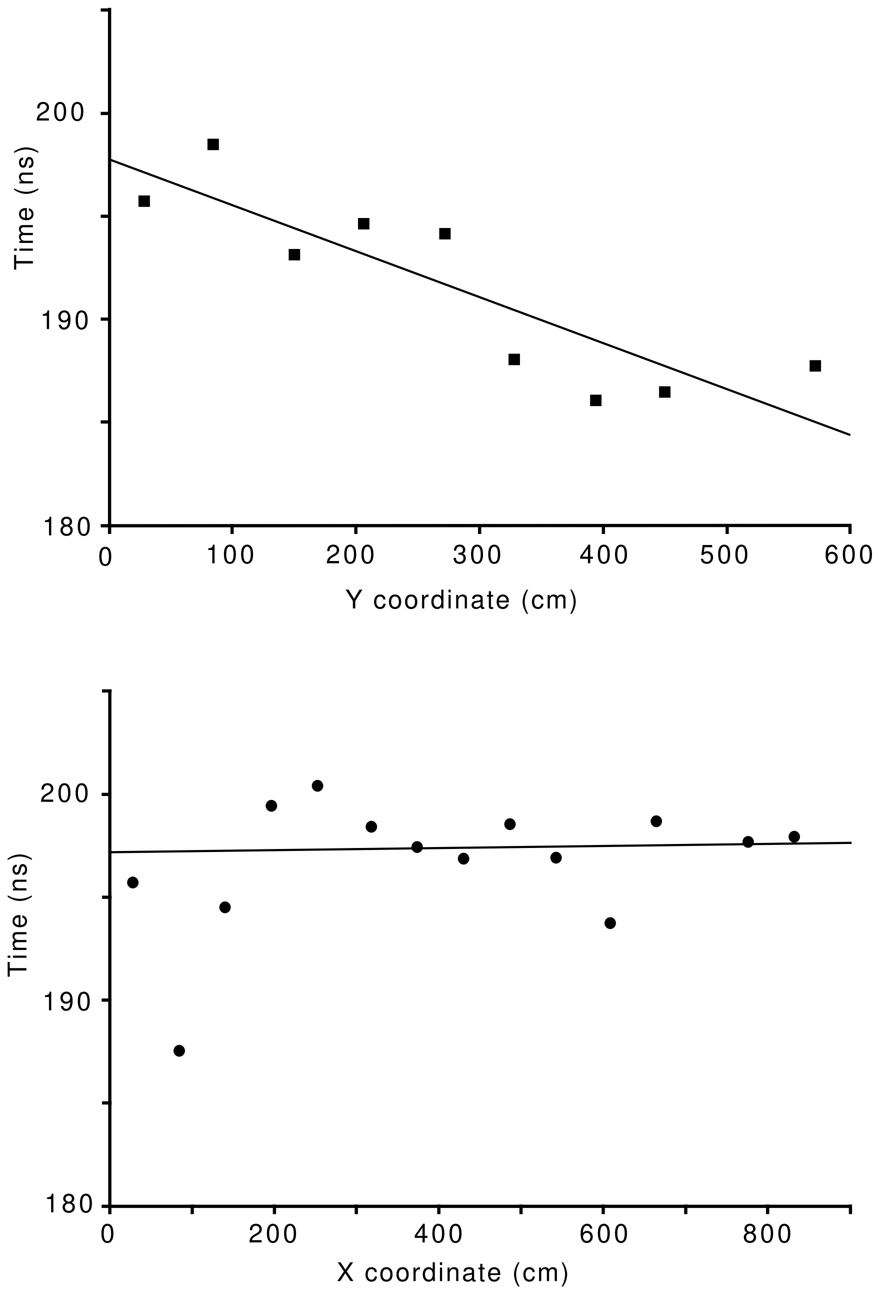

Figure 25: Time profile observed in x and y direction for one typical event. Straight lines are fit to the experimental points

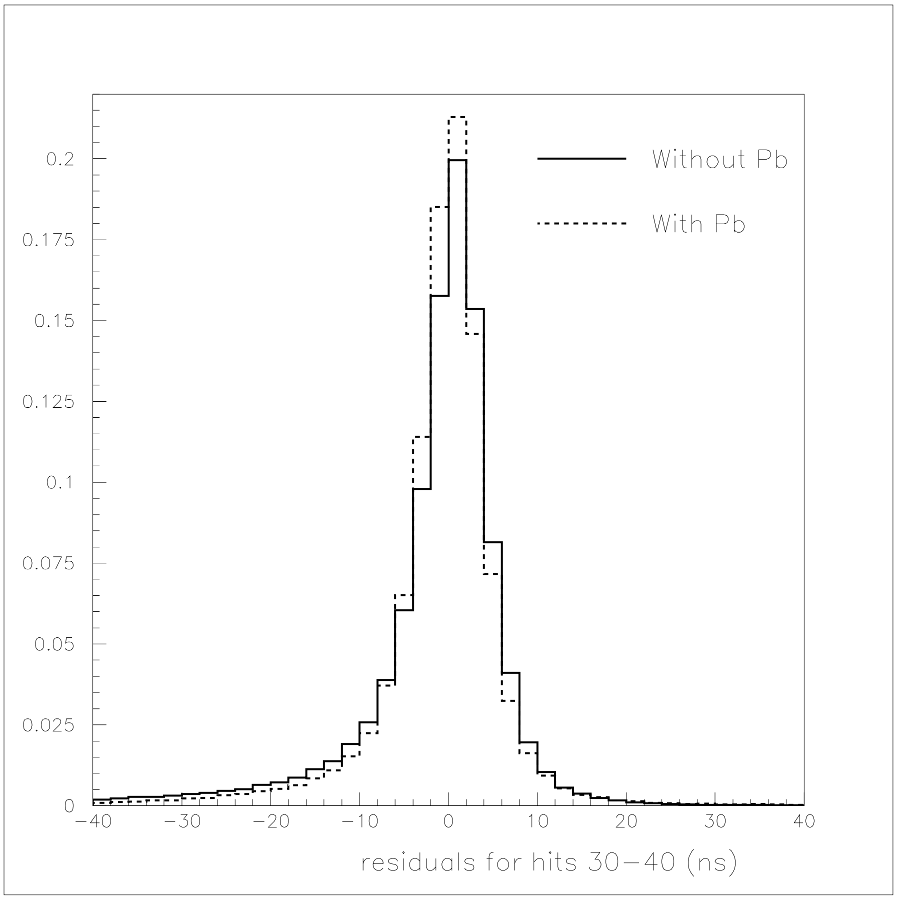

Figure 26: Residual distribution for events with pad multiplicity in the range 30–40 hits with and without lead.

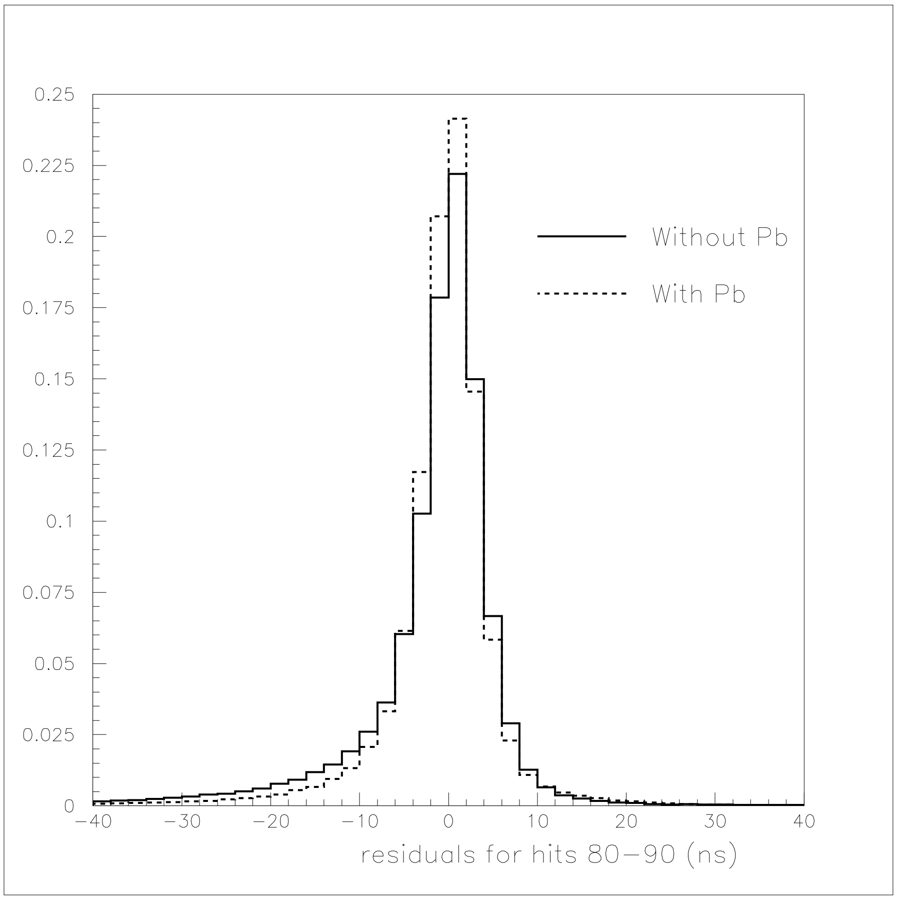

Figure 27: Residual distribution for events with pad multiplicity in the range 80–90 hits with and without lead.

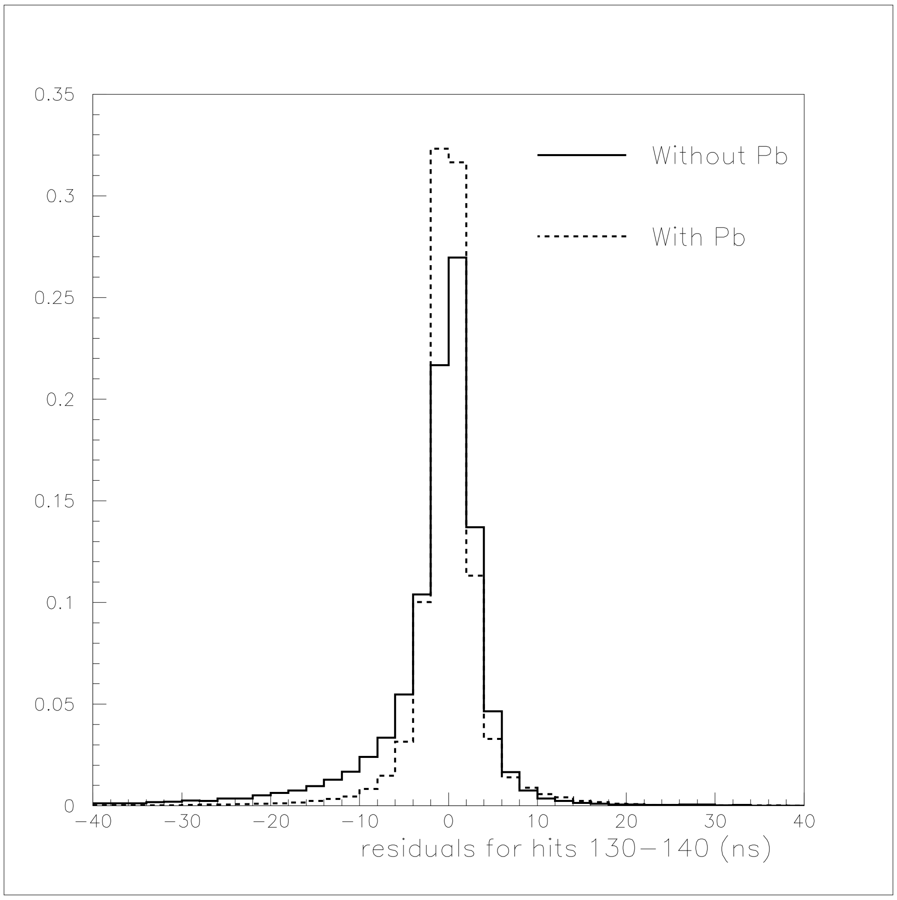

Figure 28: Residual distribution for events with pad multiplicity in the range 130–140 hits with and without lead.

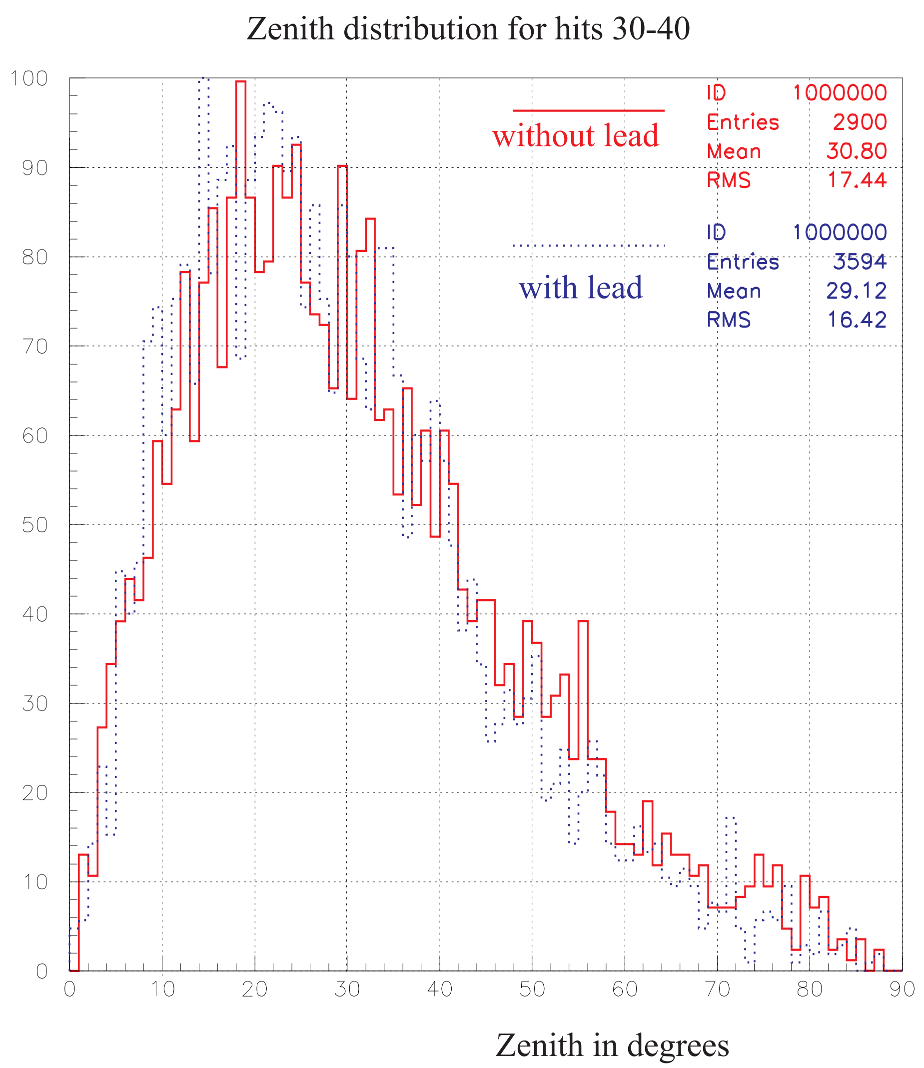

Figure 29: Zenith angle distributions with and without the 5 mm Pb layer.

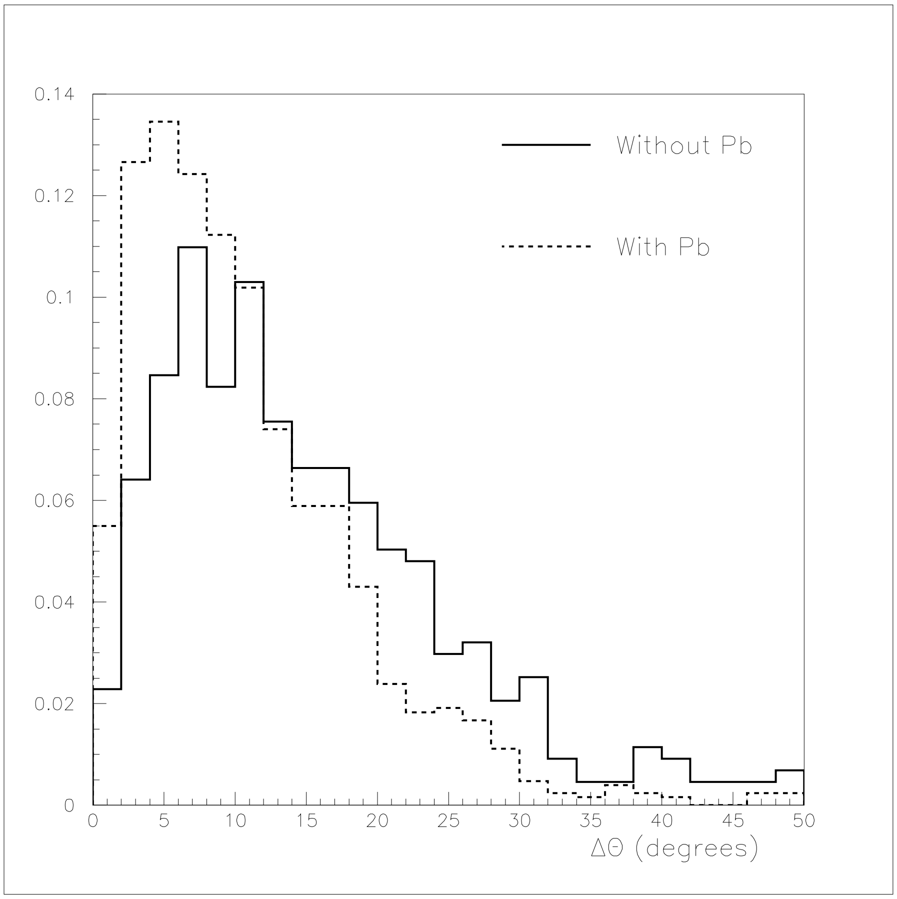

Figure 30: The space angle difference between odd numbered pads and even numbered pads for events with a total number of hits in range 130–140, with and without the 5 mm Pb layer.

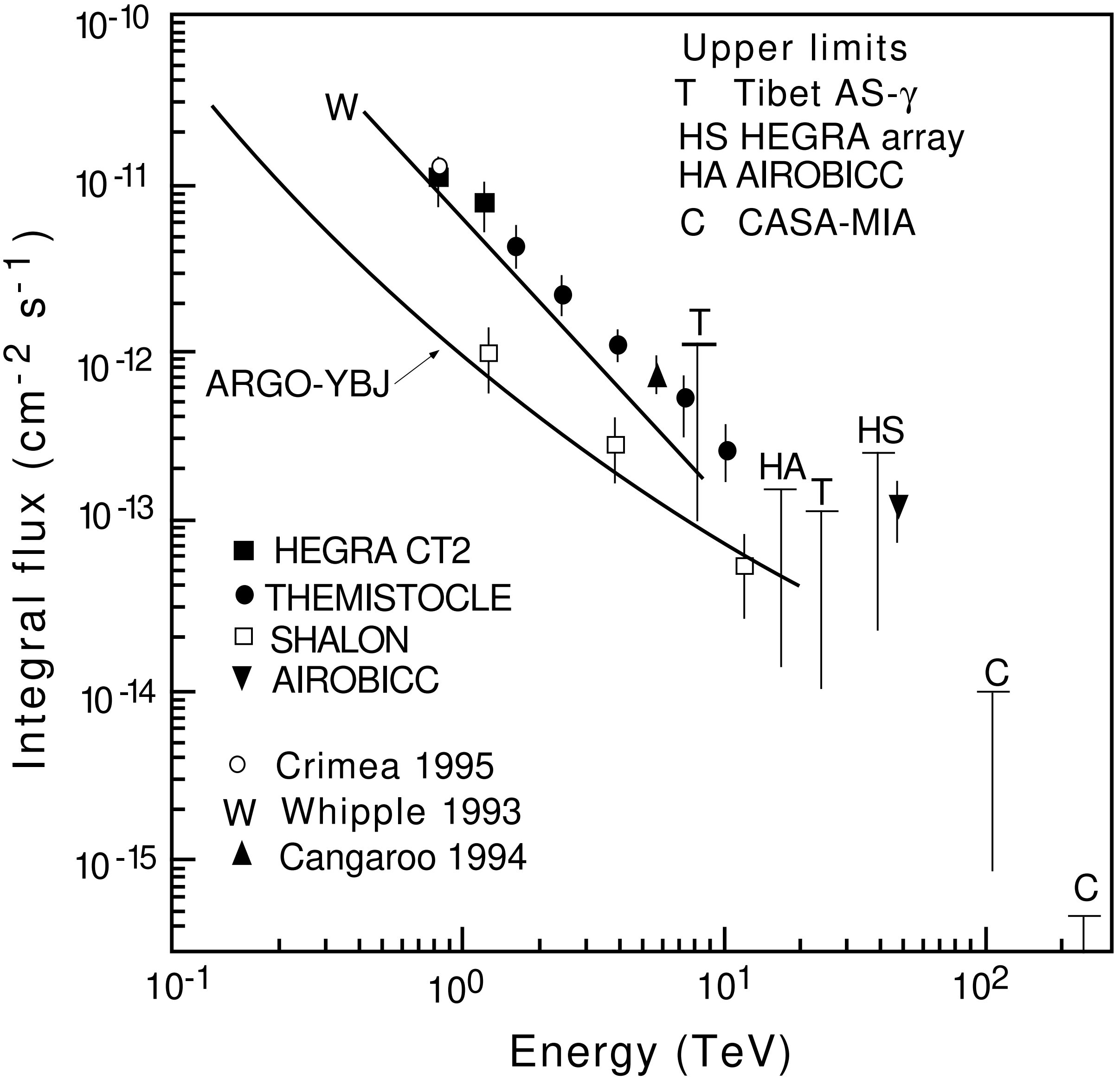

Figure 31: The expected ARGO–YBJ sensitivity to point the gamma sources compared to experimental data from Crab.

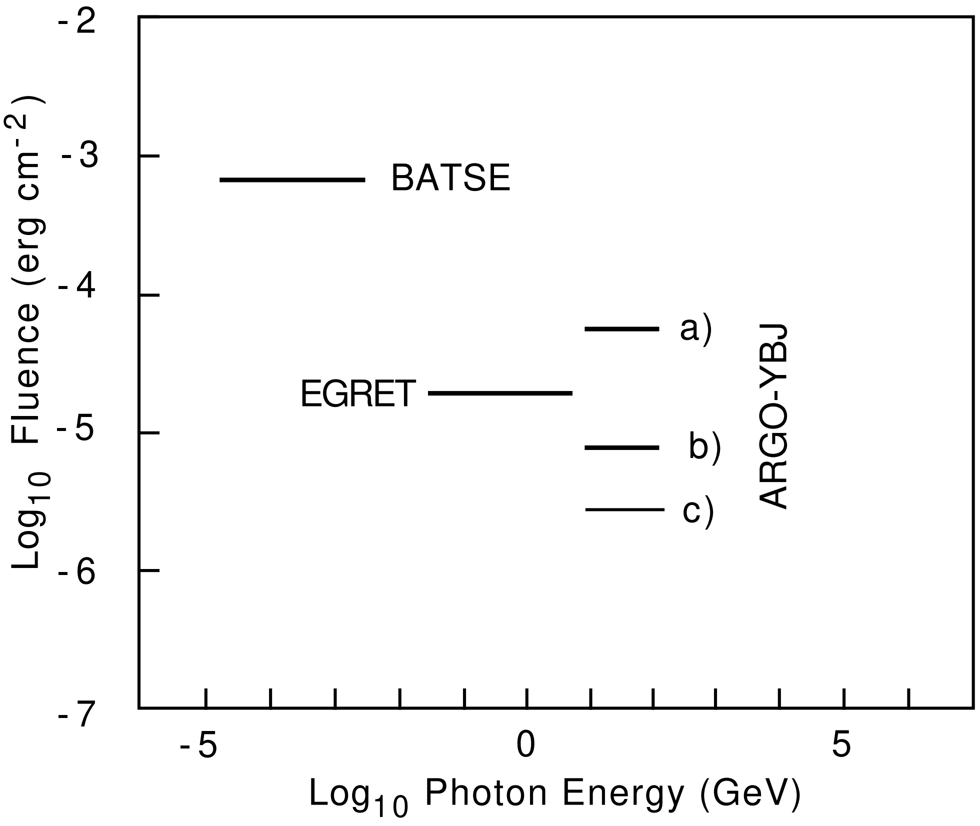

Figure 32: The minimum energy fluence, in the energy range $1 \div 100\ GeV$, detectable by ARGO–YBJ for Gamma Ray Burst of duration of 1 s. The burst spectrum is assumed to be a power law one extending in the energy range $1 \div 100\ GeV$ with spectrum slope of 3, 2 and 1 [*a), b), c)*]. In the figure are also shown the fluences measured at lower energies by BATSE and EGRET during the powerful event GRB 940217.

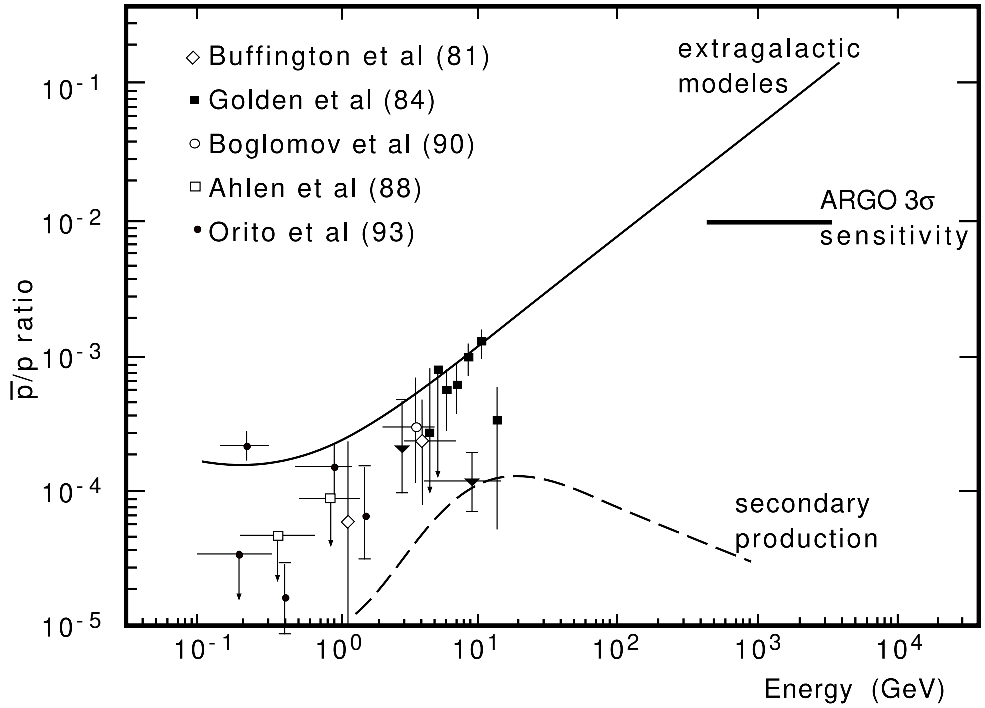

Figure 33: Upper limit at 90% c.l. on the $\bar{p}/p$ set by ARGO–YBJ in case of no signal detection

10 Conclusions

The present addendum completes a previous document in which under definite hypothesis on the detector performance, the sensitivity of the experiment to several physical processes was computed for two detector areas 3600 and 14400 m^2. The results of the experimental test performed in YBJ laboratory presented in this addendum confirm the performance of the detector (efficiency and time resolution) assumed in the sensitivity computation. Accordingly, a full coverage detector of $\sim 6500\ m^2$ (including the guard ring) is proposed. This represents a good compromise between sensitivity and cost of the experiment. We can summarize the expected performance of this detector to the most important physics goals by showing in the figures 31, 32 and 33 *i*) the sensitivity for detecting photons from point sources, *ii*) the minimum detectable fluence of 1 s GRB and *iii*) the sensitivity for measuring the antiproton–proton ratio at energies around 1 TeV.

11 Time schedule and cost estimates

TIME SCALE
We estimate that construction and assembling of the detector would be carried out according to the following time schedule:

1999 Construction of 1100 m^2 detector

2000 Assembling at YBJ and debugging of 1100 m^2 detector. Starting of data taking for GRB's detection. Construction of 1800 m^2 detector.

2001 Assembling at YBJ and debugging of 1800 m^2 detector. Construction of 2500 m^2 detector.

2002 Assembling at YBJ and debugging of 2500 m^2 detector. Starting of data taking with 5400 m^2 detector. Construction of 1100 m^2 detector for the guard ring.

2003 Assembling at YBJ and debugging of 1100 m^2 detector for the guard ring.

BUDGET ESTIMATES
The cost of the experiment will be shared between chinese and italian institutions according to the following agreement:

The chinese institutions will have in charge

1. the construction of the building and all infrastructures

2. part of the CLUSTER electronics (∼40%)

3. part of the gas system (∼50%)

4. the gas needed to run the apparatus.

The italian institution will have in charge

1. the construction of the RPC's
2. the front–end electronics and the central station electronics
3. part of the CLUSTER electronics
4. power supply (L.V. and H.V.) and distribution
5. part of the gas system
6. DAQ system
7. UPS system
8. the transportation from Italy to YBJ of all goods necessary for the experiment

Telephone link and communication via Internet will be provided by the Chinese side. A common effort will be made to establish satellite communications between Yanbajing and Chinese and Italian stations.
In the following table is reported the estimated cost in italian lira.

Item	Total cost (Glit)	1999 (Mlit)	2000 (Mlit)	2001 (Mlit)	2002 (Mlit)	2003
Building and logistic	3.50	1000	2000	500		
UPS system	0.10		25	25	50	
RPC	3.64	620	960	1320	600	140
F.E. electronics	0.42	140	140	140		
CLUSTER electronics	1.23	175	265	265	265	265
I/O and TRIG. elec.	0.16	30	75	55		
DAQ	0.27	80	90	60	40	
HV	0.14	40	50	30	20	
Gas system	0.07	25	45			
Transports	0.40		70	110	170	50
Totals	9.93	2110	3720	2505	1145	455

These cost estimates do not include missions and running expenses. The cost of the lead plates is still to be defined. According to the aforementioned commitments the cost reported in the table will be shared between Italian and Chinese sides as follows:

- Italian Institutions **5.87 Glit**
- Chinese Institutions **4.06 Glit** (2.3 MUS$)

12 APPENDIX

12.1 Gas Studies at the Yanbajing site

A preliminary study of the gas mixture at the atmospheric depth of Yanbajing (606 g/cm^2), was made with the help of a small telescope consisting of 3 RPC's of 50×50 cm^2 sensitive area with 16 read out strips 3 cm wide connected to a front–end electronics board similar to the ones used in the test carpet. The three RPC's were overlapped on one another so that clean cosmic ray signals could be detected by the triple coincidence of them. Cosmic rays were used to study the response of the RPC's to minimum ionizing particles in the peculiar temperature and pressure conditions characteristic of the mountain YBJ laboratory which represents an unprecedented environment for RPC operation. The average pressure was about 600 mbar as already said and the temperature inside the laboratory was kept between +5 and +8 C. During the test described here, which was done in the second half of February 98, the external temperature ranged between -20 and -5 ^{o}C. The telescope was oriented with the RPC's in horizontal position and the coincidence of the RPC's 1 and 3, the first and the last, was used as the signal detecting a cosmic ray crossing the RPC 2, the middle one, so that the efficiency of RPC 2 could be measured as the ratio of the triple to the double coincidences. For each gas under test a voltage scanning was done and for each voltage the counting rate and current of RPC2 were measured together with the double and triple coincidences rate. Three gases were studied, all composed of the same basic components, Tetrafluoroethane (TFE) $C_2H_2F_4$, Argon and isobutane C_4H_{10}, mixed with different proportions: TFE/Ar/i-C_4H_{10} = 45/45/10, 60/27/13 and 75/15/10 respectively. The detection efficiencies vs operating voltage for all three gases is shown in figure 34. The reduction of the amount of Argon in favor of TFE results in a clear increase of the operating voltage which is due to the increased gas density as well as to the larger quenching of the TFE. The efficiency plots in figure 34 are consistent with an increase of operating voltage of 34.2 V for a 1% reduction of the Argon. In spite of the different operating voltages all three gases exhibit a plateau efficiency of about 90%. We remark that the RPC efficiency measured on the carpet chambers is about 94% (see section 9.2). The 4% difference of the present value can be accounted by geometrical effects. Figure 35 shows the charge delivered in the gas per count of the RPC vs the operating voltage for different gas mixtures. The figure gives a clear indication that the charge decreases for decreasing amount of Argon at fixed efficiency. The lower delivered charge gives an advantage to the mixtures with higher TFE content which should be less sensitive to changes in electrode resistivity related to the laboratory temperature. A lower threshold of the front–end electronics could be required in this case.

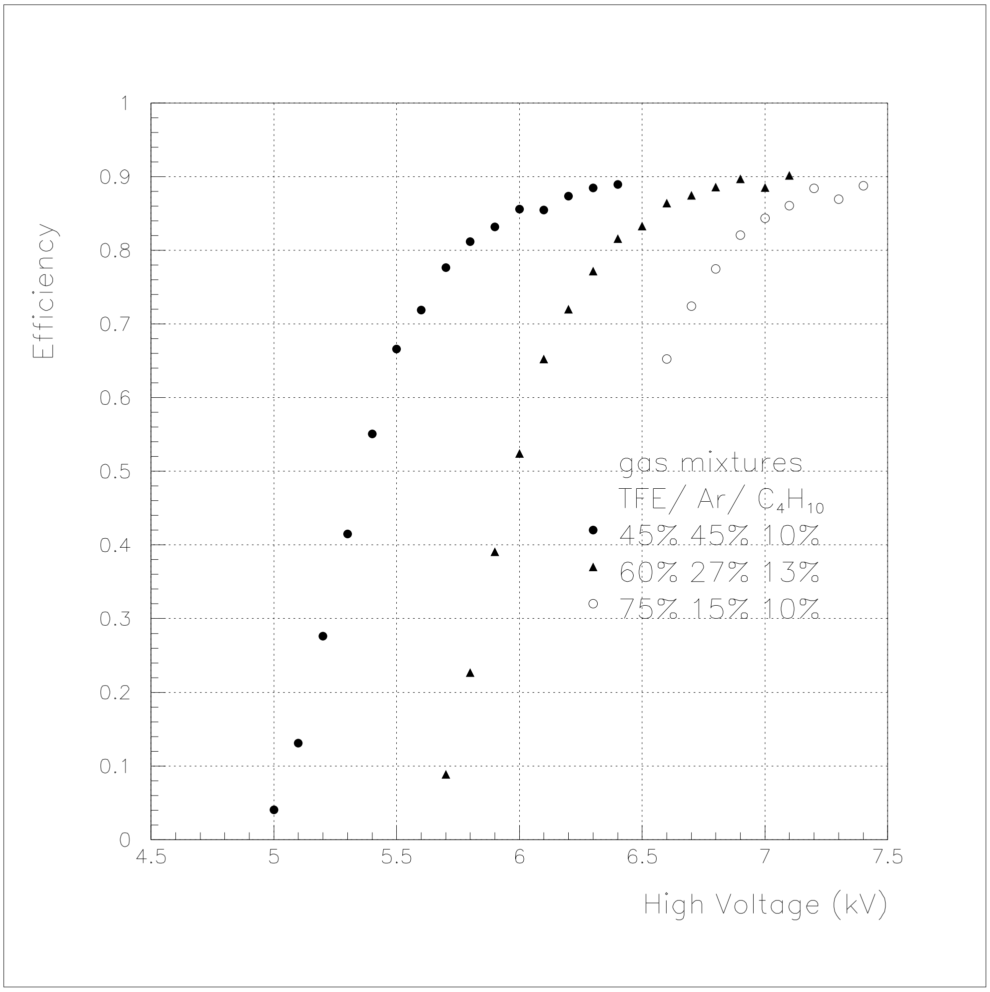

Figure 34: Plateau curves for different gas mixtures at the YBJ site

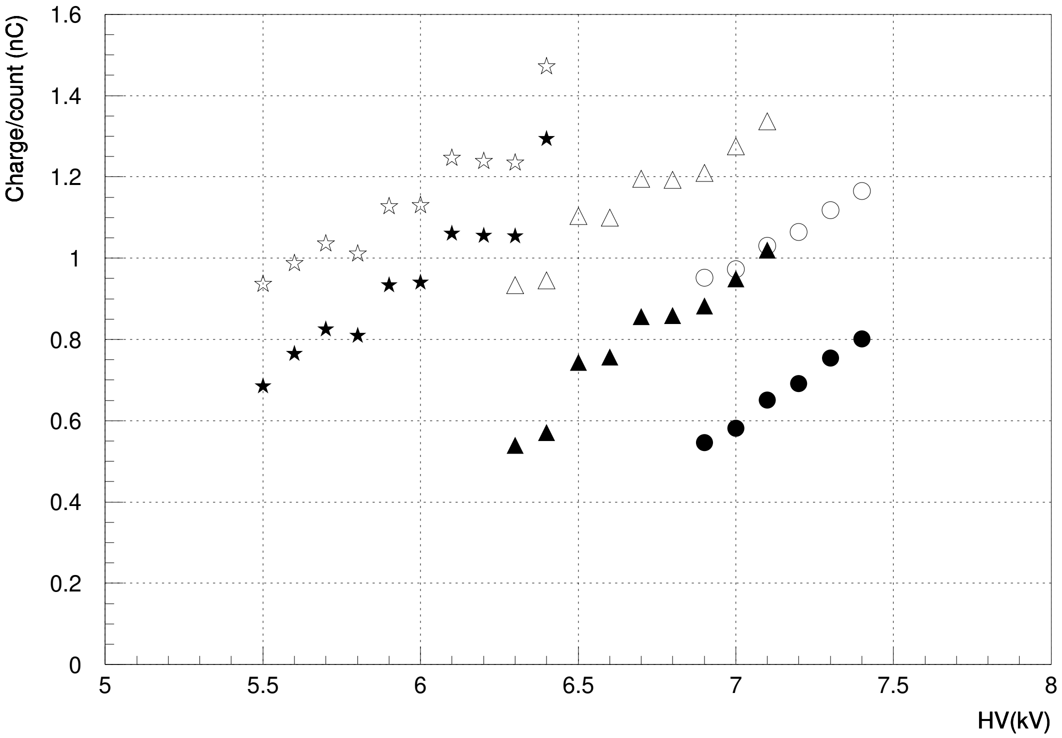

Figure 35: Current/rate for the three tested gas mixtures: TFE/Ar/C_4H_{10} 45/45/10 open star, 60/27/13 open triangle, 75/15/10 open circle. Data corresponding to full symbols are obtained by subtracting the ohmic term from the total current.

12.2 Time resolution with 6 cm wide pick–up strips

The experimental test at the YBJ site has been performed with strips 3.3 cm wide while, for the computation of sensitivity, strips 6.6 cm wide has been considered. In order to compare the performance (timing and pulse height) of an RPC system using 3 or 6 cm wide pick-up strips a small cosmic ray telescope has been built. The coincidence of three scintillator counters ($6 \times 10cm^2$, $20 \times 20cm^2$, $20 \times 20cm^2$ respectively) interspaced with $10cm$ thick lead layer defines the passing particle. Nearby and below the smallest counter an RPC chamber ($50 \times 50cm^2$) was placed. The gas mixture used in RPC was (AR 30% - ISOBUTANE 65% - FREON(R13B1) 5%), and high voltage (8500 V) was such to drive the chamber in streamer mode. To compare the behavior of 3 and 6 cm wide pick–up's on the same events, the strips were placed on both sides of the chamber (in one side the 3 cm strips and in the other side 6cm strips). The signals from the two strips were recorded by a digital, 500 Mhz oscilloscope at 500 mega–samples per second, when a trigger (telescope coincidence) occurs. The event consists of the record of the wave form (digitized) of the signal of the two strips to the same streamer discharge. An analysis has been performed by selecting the pulse height in such a way that a streamer signal is present on both strips. The time t_o when the signals cross the 30 mV threshold was estimated from data and the fluctuation of this time has been assumed as the parameter to compare the strips performance. In figure 36 the distribution of t_o is shown for both strips. The result shows a substantial equivalence, as far as the time resolution is concerned, for the 3 cm and 6 cm wide strips.

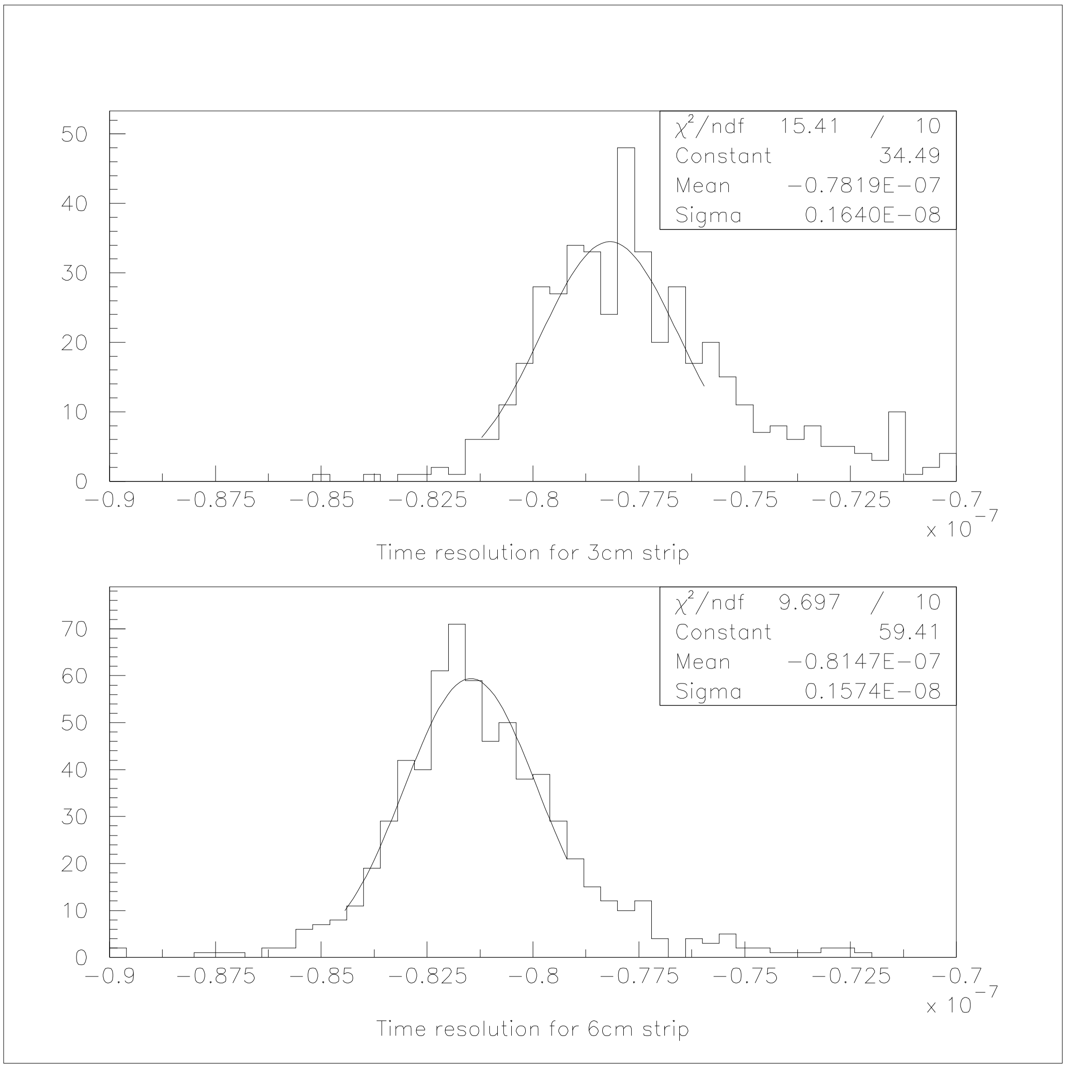

Figure 36: The time resolution for 3 and 6 cm wide pick-up strips

References

[1] ATLAS Muon Spectrometer Technical Design Report, *CERN/LHCC/97-22* (31 May 1997).

[2] R.Cardarelli et al.;, *RPC's Front-End electronics for the ATLAS LVL1 Trigger Detector*, Proc.of the 7th Pisa meeting on Advanced detectors, Isola d'Elba, May 25-31, 1997 to be published in Nucl.Instr. and Meth.

[3] M.Passaseo et al. N.I.M. A367(1995)418

[4] M.H.Salomon and F.W Stecker, Astro-ph/9704166, 1997